

AD-A047 758

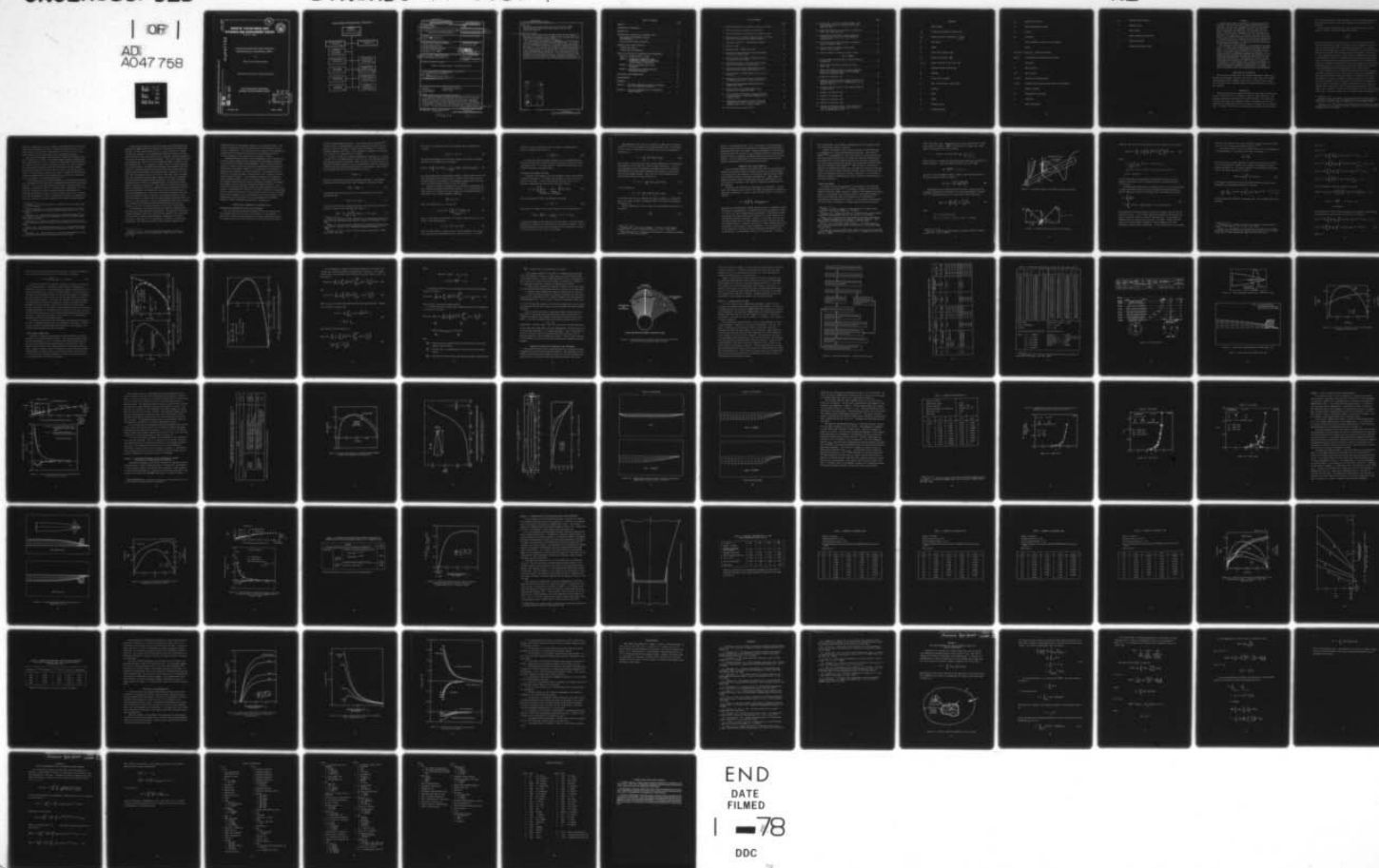
DAVID W TAYLOR NAVAL SHIP RESEARCH AND DEVELOPMENT CE--ETC F/G 13/10
A METHOD FOR PREDICTING THRUST DEDUCTION USING PROPELLER LIFTIN--ETC(U)
NOV 77 B D COX, A G HANSEN

UNCLASSIFIED

DTNSRDC-77-0087

NL

OF
AD
A047 758



12

**DAVID W. TAYLOR NAVAL SHIP
RESEARCH AND DEVELOPMENT CENTER**



Bethesda, Md. 20084

AD A047758

**A METHOD FOR PREDICTING THRUST DEDUCTION
USING PROPELLER LIFTING SURFACE THEORY**

by

Bruce D. Cox and Allen G. Hansen

APPROVED FOR PUBLIC RELEASE: DISTRIBUTION UNLIMITED

**SHIP PERFORMANCE DEPARTMENT
RESEARCH AND DEVELOPMENT REPORT**

DDC

RECEIVED
DEC 20 1977
B

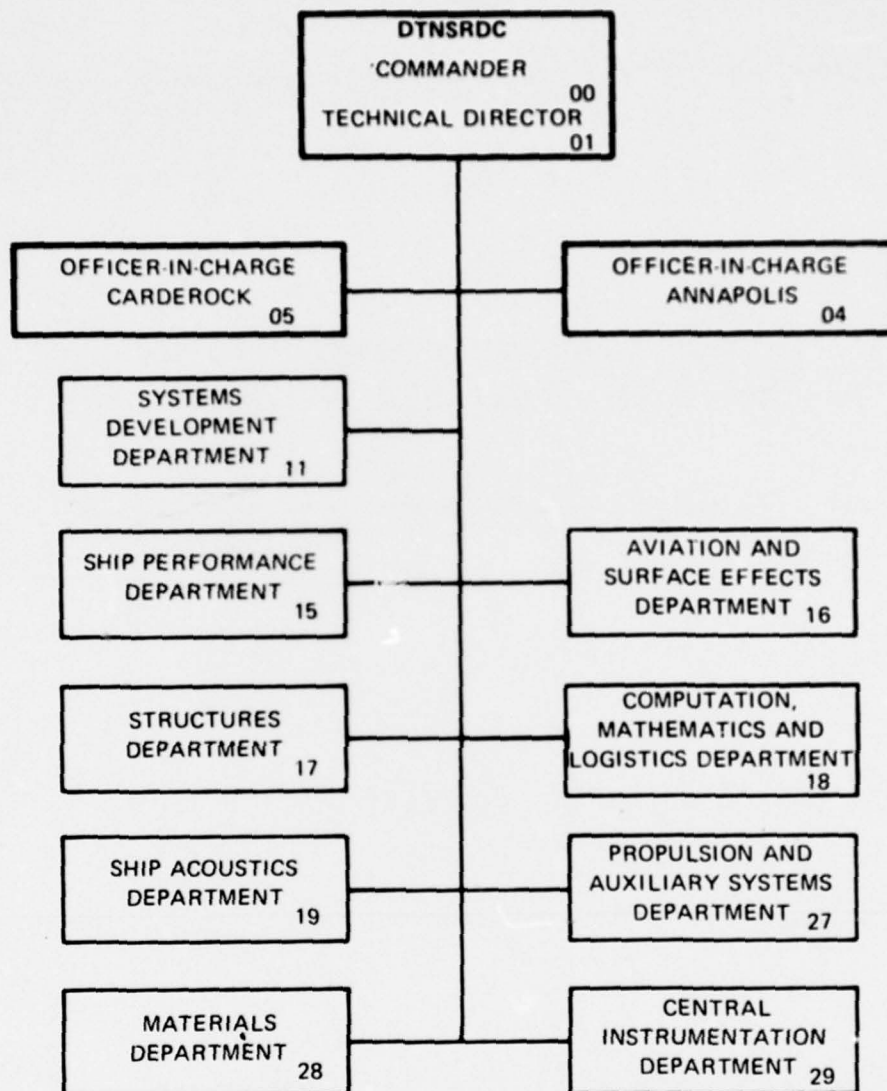
A METHOD FOR PREDICTING THRUST DEDUCTION USING PROPELLER
LIFTING SURFACE THEORY

AD No. _____
DDC FILE COPY

November 1977

Report 77-0087

MAJOR DTNSRDC ORGANIZATIONAL COMPONENTS



UNCLASSIFIED

SECURITY CLASSIFICATION OF THIS PAGE (When Data Entered)

REPORT DOCUMENTATION PAGE		READ INSTRUCTIONS BEFORE COMPLETING FORM
1. REPORT NUMBER DTNSRDC-77-0087	2. GOVT ACCESSION NO.	3. RECIPIENT'S CATALOG NUMBER
4. TITLE (and Subtitle) A METHOD FOR PREDICTING THRUST DEDUCTION USING PROPELLER LIFTING SURFACE THEORY.	5. TYPE OF REPORT & PERIOD COVERED Research and Development rept.	
7. AUTHOR(s) B.D./Cox A.G./Hansen	8. CONTRACT OR GRANT NUMBER(s)	
9. PERFORMING ORGANIZATION NAME AND ADDRESS David W. Taylor Naval Ship Research and Development Center Bethesda, Maryland 20084	10. PROGRAM ELEMENT, PROJECT, TASK AREA & WORK UNIT NUMBERS (See reverse side)	
11. CONTROLLING OFFICE NAME AND ADDRESS Naval Sea Systems Command Washington, D.C. 20362	12. REPORT DATE Nov 77	
14. MONITORING AGENCY NAME & ADDRESS (if different from Controlling Office) F61412, F43421	13. NUMBER OF PAGES 88 1284 p.	
	15. SECURITY CLASS. (of this report) UNCLASSIFIED	
16. DISTRIBUTION STATEMENT (of this Report) APPROVED FOR PUBLIC RELEASE: DISTRIBUTION UNLIMITED		
17. DISTRIBUTION STATEMENT (of the abstract entered in Block 20, if different from Report) ZF61412001, SF4342151		
18. SUPPLEMENTARY NOTES		
19. KEY WORDS (Continue on reverse side if necessary and identify by block number) Propeller Propeller-Hull Interaction Thrust Deduction Potential Flow Lifting Surface		
20. ABSTRACT (Continue on reverse side if necessary and identify by block number) An analytical method is presented for predicting the added resistance (thrust deduction) arising from propeller-hull interaction. The theory is formulated in terms of the potential flow about the hull and appendages which are represented by surface singularity distributions. The influence of the propeller is derived from lifting-surface theory including the effects of blade number, thickness, skew, rake, and radial and chordwise load distribution. In order to determine the interaction force, propeller-induced (Continued on reverse side)		

DD FORM 1 JAN 73 1473

EDITION OF 1 NOV 65 IS OBSOLETE
S/N 0102-LF-014-6601

UNCLASSIFIED

SECURITY CLASSIFICATION OF THIS PAGE (When Data Entered)

387682

Inca

UNCLASSIFIED

SECURITY CLASSIFICATION OF THIS PAGE (When Data Entered)

(Block 10)

IED funding under Element 62766N, Work Unit No. 1552-119, NAVMAT
DIRECT Laboratory Funding under Element 62543N, Work Unit Nos.
1520-004 and 1500-200.

(Block 20 Continued)

velocities and the modified hull pressure distribution are computed with appropriate corrections to the hull singularities. The axial force is then derived by integration of the pressure on the hull and also by application of the steady-flow Lagally theorem.

The usefulness of this technique is illustrated by its application to several stern propeller-body-of-revolution configurations. It is shown that stern appendages contribute up to 25 percent of the total thrust deduction. The relative contributions of propeller loading and thickness are examined. It is found that the lifting-surface representation predicts 10 to 20 percent lower thrust deduction than the classical lifting-line (sink disk) approximation. Calculations for a series of four raked propellers illustrate the significant (over 50 percent) attenuation of the interaction force as rake is increased. It is concluded that the method is useful for both the analysis of a given design and for parametric investigations of higher efficiency propeller-afterbody configurations. The method may also be extended to treat contrarotating and ducted propellers.

ACCESSION for	
NTIS	White Section <input checked="" type="checkbox"/>
DDC	Buff Section <input type="checkbox"/>
UNANNOUNCED	<input type="checkbox"/>
JUSTIFICATION	
BY	
DISTRIBUTION/AVAILABILITY CODES	
Dist. <input type="checkbox"/> <input type="checkbox"/> <input type="checkbox"/> or SPECIAL	
A	

UNCLASSIFIED

SECURITY CLASSIFICATION OF THIS PAGE (When Data Entered)

TABLE OF CONTENTS

	Page
ABSTRACT	1
ADMINISTRATIVE INFORMATION	1
INTRODUCTION	1
PROPELLER-HULL INTERACTION IN POTENTIAL FLOW	5
SINGULARITIES REPRESENTING THE HULL AND APPENDAGES	5
SOLUTION FOR THE THRUST DEDUCTION	8
PROPELLER FIELD POINT VELOCITIES	10
LIFTING-LINE THEORY	11
LIFTING-SURFACE CORRECTIONS	17
EXAMPLE CALCULATIONS AND COMPARISON WITH EXPERIMENTS	22
EXAMPLE 1: APPENDED SERIES 58 FORM	24
EXAMPLE 2: COMPARISON OF THEORETICAL AND EXPERIMENTAL PRESSURE DISTRIBUTIONS ON THREE BODIES OF REVOLUTION	32
EXAMPLE 3: BODY OF REVOLUTION WITH STERN APPENDAGES	44
EXAMPLE 4: APPENDED BODY OF REVOLUTION WITH FOUR RAKED PROPELLERS	50
CONCLUSIONS AND RECOMMENDATIONS	61
ACKNOWLEDGMENTS	65
REFERENCES	66
APPENDIX A - THE FORCE GENERATED ON A BODY IN POTENTIAL FLOW BY AN ISOLATED SINGULARITY	69
APPENDIX B - SINK DISK REPRESENTATION OF A MODERATELY LOADED PROPELLER	75

LIST OF FIGURES

	Page
1 - Coordinate Systems for Propeller Lifting Line Theory	13
2 - Force and Velocity Diagram at Lifting Line	13
3 - Field Point Velocity Calculations in Propeller Plane	18
4 - Representation of Propeller Blade by Source and Vortex Line Lines (Projected View Looking Forward)	23
5 - Interaction Analysis - Computational Procedure	25
6 - Propeller 3638	28
7 - Representation of NSRDC Model 4620	29
8 - Lifting Line Circulation and Pitch Representing Loading of Propeller 3638	30
9 - Control Points and Propeller Induced Velocities on Appended Series 58 Body	31
10 - Radial Distribution of Propeller Sink Strength Derived From Lifting Line Calculations	34
11 - Calculated Longitudinal Distribution of Thrust Deduction Force on Model 4620 (Body Only)	35
12 - Representation of DTNSRDC Models 5225-1, 5225-2, and 5225-3	36
13 - Measured and Calculated Pressure Distributions on DTNSRDC Models 5225-1, 5225-2, and 5225-3	41
14 - Profile and Quadrilateral Representation of DTNSRDC Model 5224-1	45
15 - Design Circulation and Hydrodynamic Pitch Distributions of Propeller 4567A	46
16 - Control Points and Propeller Induced Velocities on Appended Body of Revolution (DTNSRDC 5224-1) Propeller 4567A	47
17 - Longitudinal Distribution of Thrust Deduction (Cumulative From Stern) on Body of Revolution (DTNSRDC Model 5224-1, Propeller 4567A)	49
18 - Stern Alteration on Model 5224-2	51

	Page
19 - Lifting Line Circulation and Hydrodynamic Pitch Representing Loading of Propellers 4486, 4487, 4488, and 4489	57
20 - Radial Distributions of Total Rake of Propellers 4486, 4487, 4488, and 4489	58
21 - Longitudinal Distribution of Thrust Deduction (Cumulative From Stern) With Four Propellers on Body 5224-2	61
22 - Propeller Induced Axial Velocities on Appended Body of Revolution 5224-2	62
23 - Contributions to Propeller Induced Axial Velocity on Body 5224-2	63
A-1 Control Volume for Analysis of Force on Body	69

LIST OF TABLES

1 - Propeller-Body Configurations in Thrust Deduction Calculations	26
2 - Offsets and Particulars for Series 58 Form, Model 4620	27
3 - Computed and Measured Values of Thrust Deduction Fraction for Appended Series 58 Body (DTNSRDC Model 4620, Propeller 3638)	33
4 - Geometry of Propeller 4577	40
5 - Computed and Measured Thrust Deduction Fraction for Appended Body of Revolution (DTNSRDC Model 5224-1, Propeller 4567A)	48
6 - Principal Characteristics of Four Raked Propellers on Model 5224-2	52
7 - Geometry of Propeller 4486	53
8 - Geometry of Propeller 4487	54
9 - Geometry of Propeller 4488	55
10 - Geometry of Propeller 4489	56
11 - Computed and Measured Values of Thrust Deduction Fraction for Propellers 4486, 4487, 4488, and 4489 on DTNSRDC Model 5224-2	59

NOTATION

c	Chord length
C_{ij}	Coefficients defined by equation (8)
C_{Th}	Propeller thrust coefficient, $\frac{T}{\rho_2 \pi R^2 V^2}$
\vec{e}	Unit vector
f_m	Camber
\vec{F}	Fluid force acting on body
J_v	Advance coefficient, $\frac{\pi V}{\Omega R}$
J_0, J_1	Bessel functions of the first kind
L	Lift/unit radius; body length
\vec{M}	Momentum
m	Point source strength
\vec{n}	Unit vector normal to body surface
p	Pressure
P	Pitch
Q	Torque
\vec{r}	Position vector
R	Propeller radius

R_H	Propeller hub radius
R_n	Body length Reynolds number
S	Surface
R_T	Resistance
t	Thrust deduction fraction; time; thickness
T	Thrust
$\vec{u}'(x, r, \varphi) = (u'_x, u'_r, u'_\varphi)$	= Induced velocities
$\vec{u}(x, r)$	Circumferential mean induced velocities
V	Ship speed
\vec{v}	Fluid velocity
$w(r)$	Wake fraction
(x, y, z)	Cartesian coordinate system
(x, r, φ)	Cylindrical coordinate system fixed to the propeller
Z	Number of Blades
β_i	Hydrodynamic pitch angle
$\vec{\gamma}$	Vorticity
Γ	Bound circulation

δ_{ij}	Kronecker delta function
ϵ	Drag/lift ratio
ρ	Fluid density
σ	Source strength per unit area
ϕ	Velocity potential
Ω	Propeller rotational speed

ABSTRACT

An analytical method is presented for predicting the added resistance (thrust deduction) arising from propeller-hull interaction. The theory is formulated in terms of the potential flow about the hull and appendages which are represented by surface singularity distributions. The influence of the propeller is derived from lifting-surface theory including the effects of blade number, thickness, skew, rake, and radial and chordwise load distribution. In order to determine the interaction force, propeller-induced velocities and the modified hull pressure distribution are computed with appropriate corrections to the hull singularities. The axial force is then derived by integration of the pressure on the hull and also by application of the steady-flow Lagally theorem.

The usefulness of this technique is illustrated by its application to several stern propeller-body-of-revolution configurations. It is shown that stern appendages contribute up to 25 percent of the total thrust deduction. The relative contributions of propeller loading and thickness are examined. It is found that the lifting-surface representation predicts 10 to 20 percent lower thrust deduction than the classical lifting-line (sink disk) approximation. Calculations for a series of four raked propellers illustrate the significant (over 50 percent) attenuation of the interaction force as rake is increased. It is concluded that the method is useful for both the analysis of a given design and for parametric investigations of higher efficiency propeller-afterbody configurations. The method may also be extended to treat contrarotating and ducted propellers.

ADMINISTRATIVE INFORMATION

This work was performed under the in-house independent research and exploratory development program of the David W. Taylor Naval Ship Research and Development Center (DTNSRDC) (Work Unit No. 1552-119) and the High Speed Submarine Direct Laboratory Funding Program (Work Unit No. 1520-004 and 1500-200).

INTRODUCTION

The interaction force arising from propellers operating in close proximity to the ship's stern is a familiar concept to naval architects. The propeller accelerates the flow over the hull afterbody. For sufficiently fine ship forms where flow separation effects are minimal, the velocity increase and accompanying reduction in pressure increases the hull pressure drag. The higher velocity also increases the wall shear stress, and hence,

the frictional resistance. The net result is that the delivered propeller thrust must be greater than the hull resistance in the absence of the propeller.

This increase in resistance due to the propeller-hull interaction is defined in terms of the thrust deduction fraction t ,

$$t = \frac{T - R_T}{T}$$

where R_T is the bare hull resistance and T is the propeller thrust. The thrust deduction must be known in advance so that a propeller design will meet the specified propulsion requirements. One approach is to conduct model-scale propulsion tests using a stock propeller with similar principal characteristics. While this technique has proven reasonably satisfactory for many conventional designs, a large number of experiments are required to investigate the effects of different afterbody forms, propeller locations, blade geometries, and loading characteristics. Thus, an analytical prediction technique is desirable both from the standpoint of predicting the interaction force for a given propeller and hull design, and for economically investigating more efficient propeller-hull configurations.

Various techniques for the analysis and prediction of thrust deduction have been reported in the last forty years, as shown in the comprehensive bibliography presented by Nowacki and Sharma.¹ Dickman² was the first investigator to provide a reasonable theoretical analysis of the interaction force between a hull and propeller. To represent an axisymmetric body, he applied the method of discrete singularities on the body axis together with a single point sink to represent the propeller. With this model, it was possible to relate the thrust deduction to the thrust loading coefficient. During the 1940's, some of Dickman's ideas were extended, as

¹Nowacki, H. and S.D. Sharma, "Free Surface Effects in Hull Propeller Interaction," The University of Michigan College of Engineering Report 112 (Sep 1971). A complete listing of references is given on pages 66-67.

²Dickmann, H.E., "The Interaction between Propeller and Ship with Special Consideration to the Influence of Waves," Jahrbuch der Schiffbautechnischen Gesellschaft, Vol. 40 (1939).

outlined by Weinblum³ in his survey paper. Korvin-Kroukovsky⁴ also used the method of singularities, but used a constant-strength sink disk as a propeller model, and corrected the body sources to account for both the propeller induced flow and the boundary layer displacement thickness.

More recent developments have logically followed from advances in propeller theory and the advent of high-speed digital computing capabilities. Thus, Beveridge⁵ was the first to apply the Douglas-Neumann three-dimensional potential flow calculation to represent the body. In a later investigation, Beveridge⁶ introduced a sink disk with radially varying strength derived from propeller lifting-line theory. Based on this method, predictions for three different realistic hull forms, including one surface ship, compared reasonably well with experimental data. A similar technique has also been applied to contrarotating propellers.^{7,8}

In the present work, an extended treatment of the potential flow analysis is developed which differs in two fundamental respects from previous approaches. First, a more comprehensive and realistic representation of the propeller is introduced, based on a lifting-surface formulation. This overcomes the limitations of the lifting-line sink-disk approximation by including the additional effects of blade thickness, skew, rake, and chordwise load distribution. As such, the propeller calculation is comparable in scope and accuracy to currently available lifting-surface design methods.

³Weinblum, G., "The Thrust Deduction," American Society of Naval Engineers, Vol. 63 (1951).

⁴Korvin-Kroukovsky, B.V., "Stern Propeller Interaction with a Streamline Body of Revolution," International Shipbuilding Progress, Vol. 3, No. 17 (1956).

⁵Beveridge, J.L., "Pressure Distribution on Towed and Propelled Streamline Bodies of Revolution at Deep Submergence," David Taylor Model Basin Report 1665 (Jun 1966).

⁶Beveridge, J.L., "Analytical Prediction of Thrust Deduction for Submersibles and Surface Ships," Journal of Ship Research, Vol. 13, No. 4 (Dec 1969).

⁷Nelson, D.M., "Development and Application of a Lifting-Surface Design Method for Counterrotating Propellers," Naval Undersea Center TP 326 (Nov 1972).

⁸Beveridge, J.L., "Thrust Deduction in Contrarotating Propellers," Naval Ship Research and Development Center Report 4332 (Nov 1974).

In previous investigations, the thrust deduction has been derived by applying the Lagally steady-flow theorem to the propeller sink-disk singularities. In the present formulation, it is more convenient to consider the body flow directly. Thus, time-averaged propeller induced velocities and modified hull pressure distributions are computed, including appropriate corrections to the body singularity strengths. The force is then calculated by integrating the pressure and also by applying Lagally's theorem to the body singularities. It is assumed, as before, that for a given representation of the propeller, the added hull resistance arises entirely from the reduction in afterbody pressure and that this pressure distribution may be derived solely from potential flow considerations. Although it is recognized that the boundary layer at the stern is relatively thick, the potential flow formulation has been widely accepted on the basis of agreement between predicted and measured thrust deduction. Recently, wind-tunnel experiments were conducted on streamlined bodies of revolution with and without a propeller in operation.⁹ The results show that while the theory cannot satisfactorily predict the absolute pressure distributions near the stern, the difference in pressure due to the action of the propeller is predicted remarkably well. It was also found that increases in wall shear stress contribute less than 5 percent of the integrated pressure force. For these reasons, it appears that the Douglas-Neumann potential-flow calculation is a sound approach, at least for nonseparating hull forms. Moreover, the calculation of the detailed pressure distribution will serve as a necessary first step in future treatments of the viscous flow problem.

In this report, the theoretical basis and numerical techniques for predicting the thrust deduction are presented. The analysis is restricted to deeply submerged bodies, for which the hull potential flow calculation is only briefly reviewed, being extensively documented in the cited literature. (The theory can, in principle, be extended to surface ship applications; the free-surface would be approximately represented by

⁹Huang, T. et al., "Propeller/Stern/Boundary-Layer Interaction on Axisymmetric Bodies: Theory and Experiment," DTNSRDC Report 76-0113 (Dec 1976).

reflecting the hull and propeller (images) in the waterline plane.) The propeller representation and field point velocity calculations are discussed in some detail. The further analysis considers the determination of the modified hull pressure and solution for the interaction force by pressure integration and by application of Lagally's theorem.

Comparisons between theoretical and experimental thrust deduction are given for deeply submerged stern propeller body-of-revolution configurations both with and without stern appendages. These configurations were chosen for initial calculations because the body geometry characteristics afford easier computation. However, it is noted that in application to submarines and torpedoes, the thrust deduction is of great practical importance in selecting propeller characteristics (e.g., diameter) for maximum propulsive efficiency. In the examples presented, it is shown that stern appendages develop as much as 25 percent of the thrust deduction. The relative contributions of propeller loading and thickness are examined and compared with the classical lifting-line sink-disk results. It is found that lifting-surface effects reduce the thrust deduction by 10 to 20 percent. Calculations for a series of four rakes illustrate the significant (over 50 percent) attenuation of the interaction force as rake is increased. Based on these examples, it is concluded that the theory provides a useful technique for both the analysis of a given design and for parametric studies of higher efficiency propeller-hull configurations.

PROPELLER-HULL INTERACTION IN POTENTIAL FLOW

SINGULARITIES REPRESENTING THE HULL AND APPENDAGES

The propeller-hull interaction analysis rests on the computation of the potential flow about the hull in the presence of the propeller. A great deal of effort has been devoted in the past to developing accurate and computationally efficient techniques for calculating the flow about

arbitrary three-dimensional bodies. In the method of Hess and Smith,^{10,11} the body surface is approximated by planar quadrilateral elements and the solution is derived in terms of simple source distributions. A recently developed computer code¹² based on this approach is employed in the present work. Briefly, the formulation is as follows.

The body is assumed to be deeply submerged and advancing at a constant velocity, \vec{V}_∞ , in an incompressible, inviscid fluid. By considering only the time-averaged propeller disturbance field, the flow is steady relative to a Cartesian coordinate system $\vec{r} = (x, y, z)$ advancing with the body. Outside the propeller blade row and slipstream the flow is irrotational. Thus, a velocity potential $\phi(\vec{r})$ exists such that $\vec{V}(\vec{r}) = \nabla\phi(\vec{r})$ and

$$\nabla^2 \phi(\vec{r}) = 0 \quad (1)$$

where \vec{r} is outside the body and the propeller slipstream. The boundary conditions are that the velocity must be tangent to the body surface,

$$\vec{n}(\vec{r}_B) \cdot \nabla\phi(\vec{r}_B) = 0 \quad (2)$$

and approach the free stream value at a large distance from the body-propeller system

$$\nabla\phi(\vec{r}) \rightarrow \vec{V}_\infty, \text{ as } |\vec{r}| \rightarrow \infty \quad (3)$$

A solution for $\phi(\vec{r})$ which satisfies equations (1) and (3) may be written in terms of a surface source distribution, $\sigma(\vec{r}_B)$, as

$$\phi(\vec{r}) = -\frac{1}{4\pi} \oint_{S_B} \frac{\sigma(\vec{r}_B)}{|\vec{r} - \vec{r}_B|} dS(\vec{r}_B) + \vec{r} \cdot \vec{V}_\infty + \phi_p(\vec{r}) \quad (4)$$

¹⁰Hess, J.L. and A.M.O. Smith, "Calculation of Nonlifting Potential Flow About Arbitrary Three-Dimensional Bodies," Journal of Ship Research (Sep 1964).

¹¹Hess, J.L. and A.M.O. Smith, "Calculation of Potential Flow About Arbitrary Bodies," Pergamon Press, Progress in Aeronautical Sciences, Vol. 8 (1966).

¹²Dawson, C.W. and J.S. Dean, "The XYZ Potential Flow Program," NSRDC Report 3892 (Jun 1972).

Here $\phi_p(\vec{r})$ is the potential due to the propeller which satisfies the condition

$$\nabla \phi_p(\vec{r}) \rightarrow 0 \quad |\vec{r}| \rightarrow \infty \quad (5)$$

Inserting this expression for $\phi(\vec{r})$ into equation (2) yields an integral equation for the unknown source strengths

$$\frac{1}{2} \sigma(\vec{r}_B) - \frac{1}{4\pi} \oint_{S_B} \sigma(\vec{r}'_B) \vec{n}(\vec{r}_B) \cdot \nabla_{\vec{r}_B} \frac{1}{|\vec{r}_B - \vec{r}'_B|} dS(\vec{r}'_B) = \vec{n}(\vec{r}_B) \cdot [\vec{V}_\infty + \nabla \phi_p(\vec{r}_B)] \quad (6)$$

It may be observed that the propeller presents a modified onset flow to the body (right-hand side of equation (6)). Moreover, the change in source strength caused by the presence of the propeller depends only on the component of induced velocity normal to the body surface.

A numerical solution of equation (6) is obtained by representing the body surface using planar quadrilateral elements. It is assumed that the source density is constant over each element and the integral equation is replaced by a set of linear algebraic equations.

$$\sum_j \sigma_i C_{ij} = V_i \quad (7)$$

where the coefficients, C_{ij} , are given by

$$C_{ij} = \delta_{ij} \frac{1}{2} - \frac{1}{4\pi} \int_{\text{element } j} \vec{n}_i \cdot \nabla \frac{1}{|\vec{r}_{B_i} - \vec{r}_{B_j}|} dS_j \quad (8)$$

and V_i is the onset flow evaluated at a selected control point (e.g., centroid) of each quadrilateral

$$V_i = \vec{n}_i \cdot [\vec{V}_\infty + \nabla \phi_p(\vec{r}_{B_i})] \quad (9)$$

Since the coefficients C_{ij} depend only on the body geometry, the inverse matrix C_{ij}^{-1} need only be derived once for a given hull form. It is then

possible to rapidly compute the source strengths corresponding to a number of propeller onset flows as

$$\sigma_i = \sum_j C_{ij}^{-1} v_i \quad (10)$$

Once the body source strengths are known, it is straightforward to compute velocities and pressures at points on the body surface or in the surrounding field. It is also possible to determine the resultant force acting on the body as described below.

SOLUTION FOR THE THRUST DEDUCTION

In general, the influence of a stern propeller causes a net increase in the hull resistance. Two methods are available to compute the force exerted on the body. In the first approach, the axial force, F_x , is derived by integrating the pressure over the body surface,

$$F_x = \vec{e}_x \cdot \int_{S_B} \left[\begin{array}{cc} p(\vec{r}_B) & - & p(\vec{r}_B) \\ \text{with} & & \text{without} \\ \text{propeller} & & \text{propeller} \end{array} \right] \vec{n}(\vec{r}_B) dS(\vec{r}_B) \quad (11)$$

where the pressure is found from Bernoulli's equation

$$p = -\frac{\rho}{2} \vec{V} \cdot \vec{V} \quad (12)$$

The velocity is computed at the control points of each quadrilateral as

$$\vec{V}_i(\vec{r}_B) = \sum_j \frac{1}{4\pi} \sigma_j \nabla \frac{1}{|\vec{r}_{B_i} - \vec{r}_{B_j}|} \Delta S_j + \vec{V}_\infty + \nabla \phi_p(\vec{r}_{B_i})$$

A distinct advantage of this method is that the effect of body form can be determined by examining the distribution of the pressure integral. Also, a detailed knowledge of the pressure distribution is an important first step in solving the viscous flow over the afterbody.

The interaction force may also be derived by application of Lagally's theory^{13,14} for a body immersed in a steady potential flow. The solution for the force on a body due to an isolated point source is developed in Appendix A as

$$\vec{F} = - \rho \oint_{S_B} \sigma(\vec{r}_B) \vec{V}_m(\vec{r}_B) dS(\vec{r}_B) \quad (13)$$

where $\vec{V}_m(\vec{r}_B)$ is the undisturbed onset velocity generated by the singularity. This equation is also valid for a point doublet singularity. It will be shown subsequently that the propeller disturbance arises from suitable distributions of sources (blade thickness) and doublets or equivalently, line vortices (blade loading). Thus, the axial force arising from the propeller-hull interaction may be written as

$$\vec{F}_x = - \vec{e}_x \cdot \rho \oint_{S_B} \sigma(\vec{r}_B) \nabla \phi_p(\vec{r}_B) dS(\vec{r}_B) \quad (14)$$

or in discrete form

$$F_x = - \vec{e}_x \cdot \sum_i \sigma_i(\vec{r}_B) \nabla \phi_{p_i}(\vec{r}_B) \Delta S_i(\vec{r}_B) \quad (15)$$

If only the total force is required, this form is simpler for computation and, in any case, provides a convenient check in the numerical evaluation of equation (11).

Once the interaction force is found, the thrust deduction fraction, t , is given by

$$t = \frac{F_x}{T} \quad (16)$$

¹³Cummins, W.E., "The Force and Moment on a Body in a Time-Varying Potential Flow," Journal of Ship Research, Vol. 1, No. 1 (Apr 1957).

¹⁴Milne-Thomson, L.M., "Theoretical Hydrodynamics," The Macmillan Company, New York, N.Y., 2nd edition (1950).

where T is the propeller thrust. Up to this point, it has been assumed that the propeller has been represented by an appropriate distribution of singularities external to the body. Within the framework of the potential flow formulation, the solution to the interaction problem is derived completely in terms of propeller disturbance velocities at points on the body surface. It is now appropriate to set forth the theoretical basis and numerical techniques for calculating these velocities.

PROPELLER FIELD POINT VELOCITIES

In the foregoing analysis, the modified body flow in the presence of a propeller is derived in terms of induced velocities on the body boundary. It is primarily in the treatment of the propeller that the present interaction analysis differs from earlier investigations. Owing largely to advances in design theory and high-speed computing capabilities, it has been possible to introduce a more realistic analytical representation of the propeller.

Previously, the propeller was approximated as a sink disk. In that model, the diameter, axial location, and radial distribution of loading are explicitly represented. In fact, as will be shown shortly, a sink disk of strength

$$\sigma(r) = \frac{Z}{2\pi} \int_r^R \frac{d\Gamma}{dr'} \frac{1}{r' \tan \beta_1(r')} dr'$$

generates the circumferential average velocity field of a moderately loaded lifting-line representation of a propeller with bound circulation Γ , pitch $2\pi r \tan \beta_1(r)$, and Z symmetrically spaced blades. Beveridge⁶ has demonstrated that this model satisfactorily predicts the thrust deduction for conventional propeller geometries. However, it is evident that this simplification breaks down for raked propellers in which the blade sections are displaced axially. Moreover, the effects of blade thickness and finite chordlength, while perhaps of small consequence to the thrust deduction, may be important to the body pressure distribution and boundary layer characteristics in the immediate vicinity of the propeller. In view of

these limitations, a more complete representation of the propeller based on lifting surface theory is required.

A number of propeller lifting surface theories have been developed and programmed for computer-aided design calculations. The method of Kerwin^{15,16} is representative of the state-of-the-art and was selected for the present application because the theory and numerical techniques have been extended to calculate induced velocities at arbitrary field points. Free space pressure predictions based on this method show excellent agreement with experimental measurements.¹⁷ Both the theory and numerical analysis are conveniently divided into a lifting-line analysis and lifting-surface corrections arising from blade thickness, blade location (skew and rake), and chordwise variation in loading. Therefore, it is possible to examine the separate contributions of various propeller characteristics to the thrust deduction.

LIFTING-LINE THEORY

The basis of analytical propeller design methods is the moderately loaded lifting line theory.^{18,19} The analysis considers the flow field associated with the steady loading on a propeller with symmetrically spaced blades. In accordance with circulation theory, the pressure loading on the blades arising from camber and incidence can be represented by distributions of bound and free vorticity. In the lifting line approximation, each blade is replaced by a single concentrated vortex line with

¹⁵Kerwin, J.E. and R. Leopold, "A Design Theory for Subcavitating Propellers," Transactions SNAME, Vol. 72 (1964).

¹⁶Kerwin, J.E., "Computer Technique for Propeller Blade Section Design," International Shipbuilding Progress, Vol. 20, No. 227 (Jul 1973).

¹⁷Denny, S.B., "Comparisons of Experimentally Determined and Theoretically Predicted Pressures in the Vicinity of a Marine Propeller," Naval Ship Research and Development Center Report 2349 (May 1967).

¹⁸Lerbs, H.W., "Moderately Loaded Propellers with Finite Numbers of Blades and an Arbitrary Distribution of Circulation," Transactions SNAME, Vol. 60 (1952).

¹⁹Morgan, W.B. and J.W. Wrench, "Some Computational Aspects of Propeller Design," Methods in Computational Physics, Vol. 4, Academic Press Inc., New York, N.Y. (1965).

bound circulation, $\Gamma(r)$. Conservation of vorticity requires that a free-vortex sheet of strength $-\frac{d\Gamma(r)}{dr}$ is shed from each lifting line. These sheets are assumed to lie on the surfaces

$$x(r, \varphi) = r \tan \beta_i(r) [\varphi - \varphi_k] \quad R_H \leq r \leq R \\ k = 1, 2, \dots, Z$$

where (x, r, φ) is a cylindrical coordinate system fixed to the propeller as shown in Figure 1. φ_k is the angular position of the k^{th} blade,

$$\varphi_k = \frac{2\pi(k-1)}{Z} \quad k = 1, 2, \dots, Z$$

and $\beta_i(r)$ is the flow angle defined in terms of the relative velocity at the blade section as shown in Figure 2.

$$\tan \beta_i(r) = \frac{V_a(r) + u'_x(0, r, \varphi_k)}{\Omega r - u'_\varphi(0, r, \varphi_k)} \quad (20)$$

Expressions for the induced velocity $\vec{u}'(x, r, \varphi) = (u'_x, u'_r, u'_\varphi)$ can be derived by applying the Biot-Savart law to the distributions of vorticity.^{15,20} The induced velocity due to the bound vortex lines, \vec{u}'_B , is

$$\vec{u}'_B(x, r, \varphi) = \sum_{k=1}^Z \frac{1}{4\pi} \int_{R_H}^R \Gamma(\rho) \frac{\vec{e}_\rho \times \vec{D}_\rho}{|\vec{D}_\rho|^3} d\rho \quad (21)$$

where

$$\vec{e}_\rho = (0, \cos \varphi_k, \sin \varphi_k) \\ \vec{D}_\rho = (x, r \cos \varphi - \rho \cos \varphi_k, r \sin \varphi - \rho \sin \varphi_k)$$

²⁰ Wu, T.Y., "Some Recent Developments in Propeller Theory," Schiffstechnik, Vol. 9, No. 47 (1962).

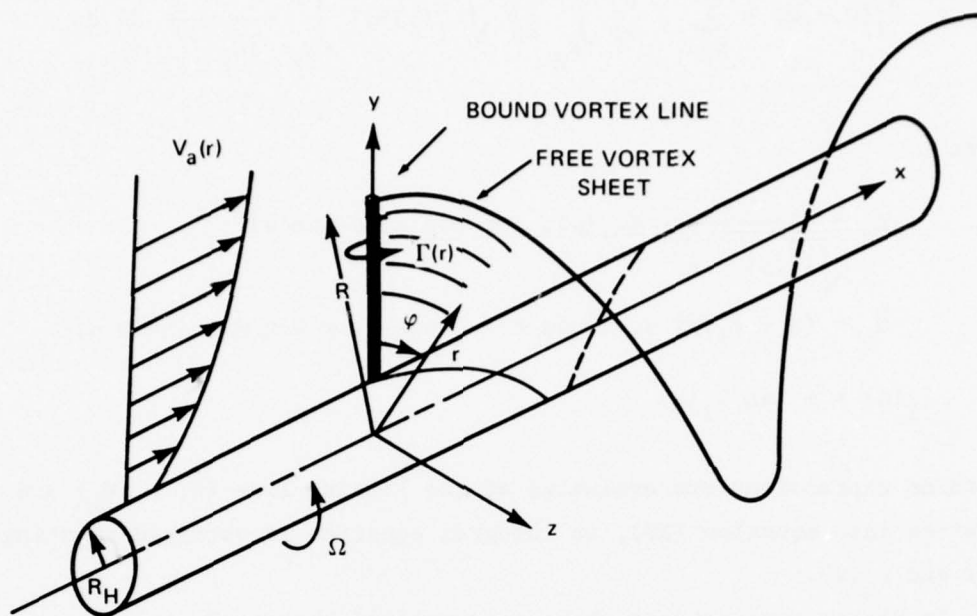


Figure 1 - Coordinate Systems for Propeller Lifting Line Theory

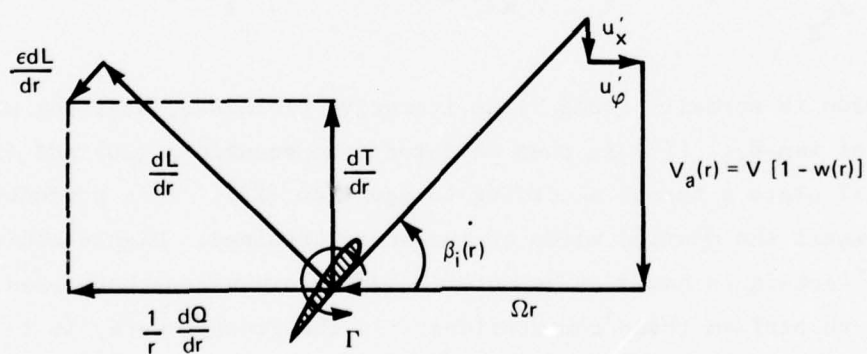


Figure 2 - Force and Velocity Diagram at Lifting Line

Similarly, the velocity induced by the free-vortex sheets, \vec{u}_T' , is given by

$$\vec{u}_T'(x, r, \varphi) = \sum_{k=1}^Z -\frac{1}{4\pi} \int_{R_H}^R \frac{d\Gamma}{d\rho} \sqrt{\lambda_i^2(\rho) + \rho^2} \int_{\varphi_k}^{\infty} \frac{\vec{e}_s \times \vec{D}_s}{|\vec{D}_s|^3} d\alpha d\rho \quad (22)$$

where

$$\vec{e}_s = \frac{1}{\sqrt{\lambda_i^2(\rho) + \rho^2}} (\lambda_i(\rho), -\rho \cos \alpha, \rho \sin \alpha)$$

$$\vec{D}_s = (x - \lambda_i(\rho) \alpha, r \cos \varphi - \rho \cos \alpha, r \sin \varphi - \rho \sin \alpha)$$

$$\lambda_i(\rho) = \rho \tan \beta_i(\rho)$$

If these expressions are evaluated at the lifting line $(0, r, \varphi_k)$ and inserted into equation (20), an integral equation is obtained relating $\Gamma(r)$ and $\beta_i(r)$.

In design applications where a prescribed thrust, T , is to be developed, a second relationship can be derived by applying the Kutta-Joukowski law (with an empirical correction for profile drag - (see Figure 2) yielding

$$\begin{aligned} T &= Z \int_{R_H}^R \frac{dT}{dr} dr \\ &= \rho Z \int_{R_H}^R \Gamma(r) [\Omega r - u_{\varphi}(0, r, \varphi_k)] [1 - \epsilon(r) \tan \beta_i(r)] dr \end{aligned} \quad (23)$$

The solution is normally found by an iterative procedure, starting with an estimate of $\tan \beta_i$. $\Gamma(r)$ is then computed from equations (20) and (22) and used to calculate a thrust according to equation (23). This procedure is repeated until the desired value of thrust is obtained. Highly efficient numerical techniques based on asymptotic series expansions have been developed to perform these computations. In the present work, it is assumed

that both $\Gamma(r)$ and $\beta_i(r)$ have been determined, either from design calculations or from a separate performance prediction.^{21,22}

The induced velocity varies with angular position, φ , corresponding to a time dependence in a reference frame fixed to the hull, i.e.,

$$\frac{\partial}{\partial \varphi} = \frac{1}{\Omega} \frac{\partial}{\partial t}$$

By virtue of the propeller symmetry, the induced velocity may be resolved into a time-averaged or steady velocity $\vec{u}(x, r)$ and harmonics in blade passage frequency, $Z\Omega$. The steady component or zero harmonic which gives rise to the thrust deduction, is given by

$$\vec{u}(x, r) = \frac{1}{2\pi} \int_0^{2\pi} \vec{u}'(x, r, \varphi) d\varphi \quad (24)$$

The separate contributions from the bound and trailing vorticity can be determined by introducing expressions of the type

$$\frac{1}{|\vec{D}_\rho|} = \sum_{n=0}^{\infty} \epsilon_n \cos n(\varphi - \varphi_k) \int_0^{\infty} J_n(kr) J_n(k\rho) e^{-k|x|} dk \quad \begin{matrix} \epsilon_n = 1 & n = 0 \\ \epsilon_n = 2 & n > 0 \end{matrix}$$

and performing the integration in equation (24). The following results are obtained:

²¹Cummings, D.E., "Numerical Prediction of Propeller Characteristics," Journal of Ship Research, Vol. 17, No. 1 (Mar 1973).

²²Tsao, S.S., "Documentation of Programs for the Analysis of Performance and Spindle Torque of Controllable Pitch Propellers," Mass. Inst. of Technology, Dept of Ocean Engineering, Report No. 75-8 (May 1975).

$$u_{B_x}(x, r) = 0$$

$$u_{B_r}(x, r) = 0$$

$$u_{B_\varphi}(x, r) = \pm \frac{Z}{4\pi} \int_{R_H}^R \frac{d\Gamma}{d\rho} \int_0^\infty J_0(k\rho) J_1(kr) e^{-k|x|} dk d\rho \quad x \gtrless 0$$

$$u_{T_x}(x, r) = - \frac{Z}{4\pi} \int_{R_H}^R \frac{d\Gamma}{d\rho} \frac{\rho}{\lambda_i(\rho)} \int_0^\infty dk J_0(kr) J_1(k\rho) \frac{e^{kx}}{2-e^{-kx}} dk d\rho \quad x \gtrless 0$$

$$u_{T_r}(x, r) = \frac{Z}{4\pi} \int_{R_H}^R \frac{d\Gamma}{d\rho} \frac{\rho}{\lambda_i(\rho)} \int_0^\infty dk J_1(kr) J_1(k\rho) e^{-k|x|} dk d\rho$$

$$u_{T_\varphi}(x, r) = - \frac{Z}{4\pi} \int_{R_H}^R \frac{d\Gamma}{d\rho} \int_0^\infty dk J_0(k\rho) J_1(kr) \frac{e^{kx}}{2-e^{-kx}} \quad x \gtrless 0$$

(25)

The total tangential velocity component is given by

$$u_\varphi(x, r) = u_{B_\varphi} + u_{T_\varphi} = \frac{Z}{4\pi} \int_{R_H}^R \frac{d\Gamma}{d\rho} \int_0^\infty J_0(k\rho) J_1(kr) \begin{Bmatrix} 0 \\ -2 \end{Bmatrix} dk d\rho \quad x \gtrless 0$$

or

$$u_\varphi(x, r) = - \frac{Z\Gamma(r)}{2\pi r} \quad x > 0, R_H \leq r \leq R$$

= 0 elsewhere

It follows that the steady velocity induced by a moderately loaded lifting line propeller at points *outside the slipstream* is given by

$$u_x(x, r) = \mp \frac{Z}{4\pi} \int_{R_H}^R \frac{d\Gamma}{d\rho} \frac{\rho}{\lambda_i(\rho)} \int_0^\infty dk J_0(kr) J_1(k\rho) e^{-k|x|} dk d\rho \quad x \gtrless 0$$

$$u_r(x, r) = \frac{Z}{4\pi} \int_{R_H}^R \frac{d\Gamma}{d\rho} \frac{\rho}{\lambda_i(\rho)} \int_0^\infty dk J_1(kr) J_1(k\rho) e^{-k|x|} dk d\rho$$

(26)

$$u_\varphi(x, r) = 0$$

and arises solely from the trailing-vortex sheets. As shown in Appendix B, this is also the velocity field due to a sink disk of strength

$$\sigma(r) = \frac{Z}{2\pi} \int_r^R \frac{d\Gamma}{d\rho} \frac{1}{\lambda_1(\rho)} d\rho = -2u_x(0,r) \quad (27)$$

The method of Kerwin,¹⁵ originally developed to compute all harmonics of the induced velocity, is based on a direct numerical integration of equations (21) and (22). The continuous-vortex sheet is divided into a set of discrete helical vortex lines of constant strength. For computational efficiency, the integration interval is divided into segments of increasing size with distance from the field point and evaluated using a five-point Gauss integration formula. The velocity is evaluated at a selected number of angular positions between two blades and resolved into blade frequency harmonics by Fourier analysis. Only the zero harmonic is used in the present application. As an example of the numerical accuracy of this method, a comparison between the computed and exact solutions of the axial velocity at the propeller disk plane for two selected loading distributions are shown in Figure 3. The velocity computed *at the lifting line* is also shown for comparison with the circumferential average.

At distances greater than about one radius, the propeller disturbance velocity is generated essentially by the lifting-line sink disk. In order to more accurately derive the near-field influence of the propeller, the lifting-surface representation must be applied.

LIFTING-SURFACE CORRECTIONS

Propeller lifting-surface analyses have been developed as a logical extension of thin planar hydrofoil theory. Thus, blade loading and thickness are represented in terms of vorticity and source-sink distributions located on a reference surface approximating the actual blade. This is normally taken to be the pitch surface derived from lifting-line calculations. Within the blade outline a distribution of bound and free vorticity is established to represent both the radial and chordwise load variation. A free-vortex sheet, previously assumed to be shed from the lifting line, now originates from the blade trailing edge.

Figure 3 - Field Point Velocity Calculations in Propeller Plane

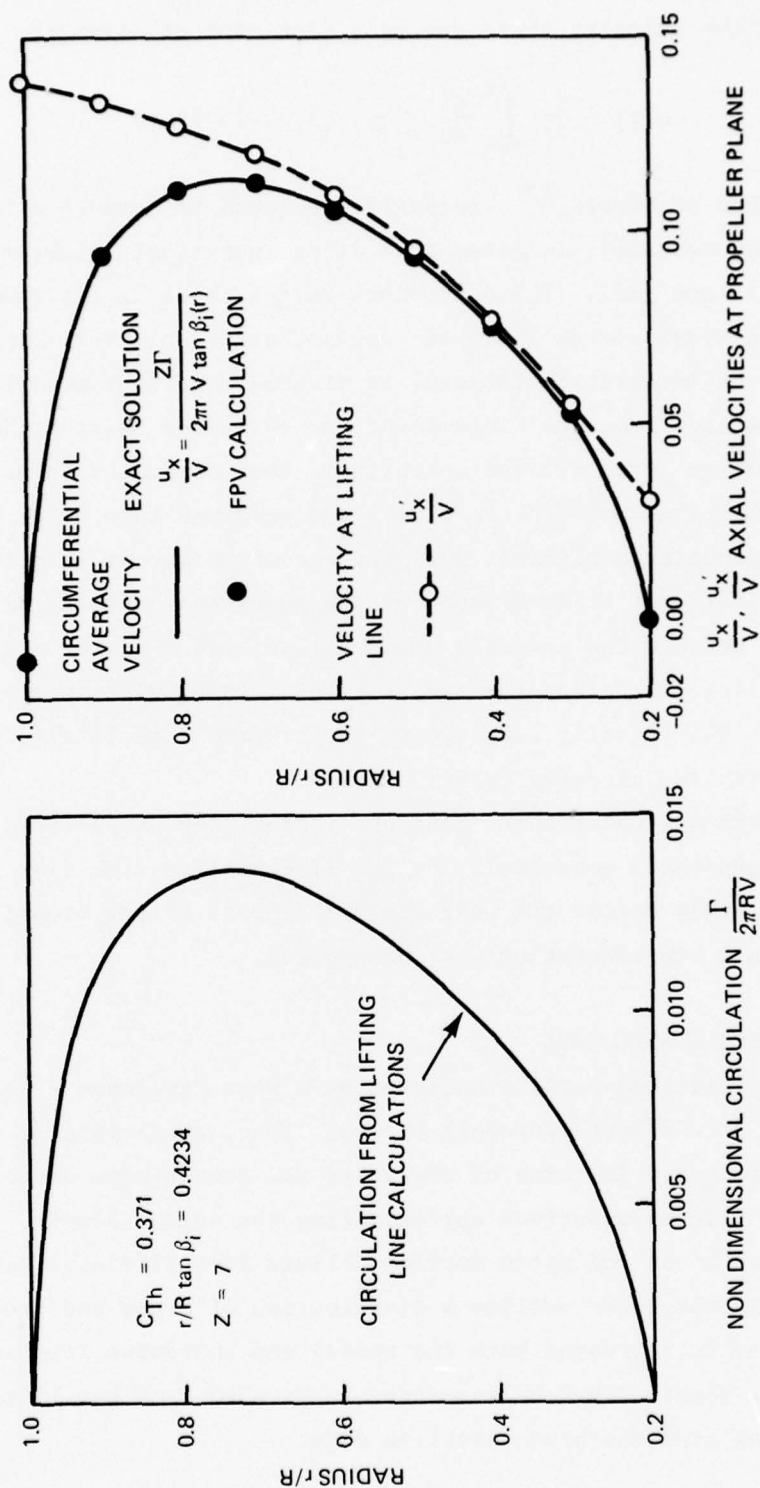


Figure 3a - Comparison of Field Point Velocity Computations With
Exact Solution for $\frac{r}{R} \tan \beta_i(r) = 0.4234$ (Constant Pitch)

Figure 3 (Continued)

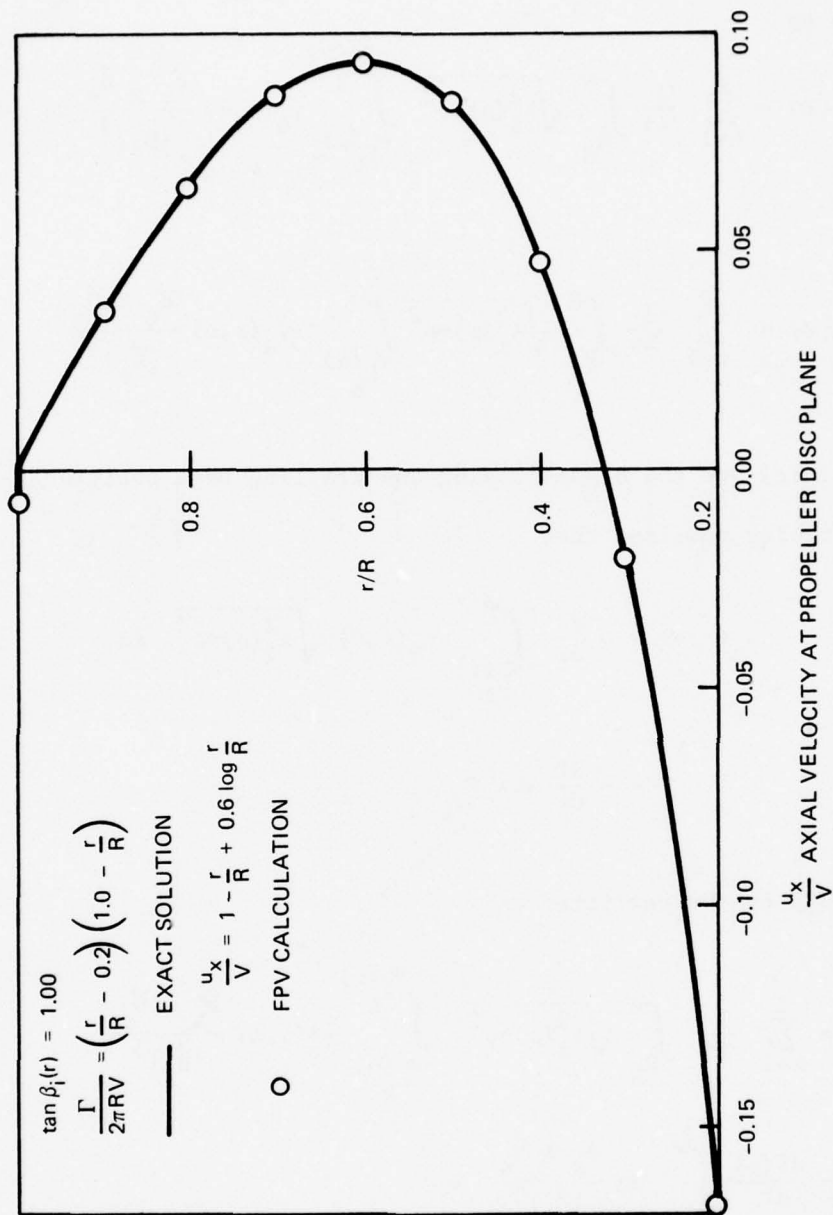


Figure 3b - Comparison of Field Point Velocity Computations With Exact Solution for $\tan \beta_i(r) = 1.0$ (Variable Pitch)

It is convenient to consider the induced velocities as the sum of the lifting-line result and separate lifting-surface corrections. The induced velocity due to the bound and free vorticity, $\vec{e}_r \gamma_B(r, \varphi)$ and $\vec{e}_s \gamma_s(r, \varphi)$, may be written as

$$\vec{u}_B(x, r, \varphi) = \sum_{k=1}^Z \frac{1}{4\pi} \int_{R_H}^R \sqrt{\lambda_i^2(\rho) + \rho^2} \int_{\varphi_{L_k}(\rho)}^{\varphi_{T_k}(\rho)} \gamma_B(\rho, \alpha) \frac{\vec{e}_\rho \times \vec{D}_s}{|\vec{D}_s|^3} d\rho d\alpha \quad (28)$$

and

$$\vec{u}_T(x, r, \varphi) = \sum_{k=1}^Z \frac{1}{4\pi} \int_{R_H}^R \sqrt{\lambda_i^2(\rho) + \rho^2} \int_{\varphi_{L_k}(\rho)}^{\infty} \gamma_s(\rho, \alpha) \frac{\vec{e}_s \times \vec{D}_s}{|\vec{D}_s|^3} d\alpha \quad (29)$$

where $\varphi_{L_k}, \varphi_{T_k}(r)$ are the blade leading and trailing edge positions. Continuity of vorticity requires that

$$\begin{aligned} \gamma_s(r, \varphi) &= -\frac{d}{dr} \int_{\varphi_{L_R}(r)}^{\varphi} \gamma_B(r, \alpha) \sqrt{\lambda_i^2(\rho) + \rho^2} d\alpha \\ &= -\frac{d\Gamma}{dr} \quad \varphi > \varphi_{T_k} \end{aligned} \quad (30)$$

and hence \vec{u}_T , can be rewritten as

$$\begin{aligned} \vec{u}_T(x, r, \varphi) &= \sum_{k=1}^Z \frac{1}{4\pi} \int_{R_H}^R \sqrt{\lambda_i^2(\rho) + \rho^2} \int_{\varphi_{L_k}(\rho)}^{\varphi_{T_k}(\rho)} \gamma_s^*(\rho, \alpha) \frac{\vec{e}_s \times \vec{D}_s}{|\vec{D}_s|^3} d\alpha \\ &\quad - \frac{d\Gamma(r)}{dr} \int_{\varphi_k}^{\infty} d\alpha \frac{\vec{e}_s \times \vec{D}_s}{|\vec{D}_s|^3} \end{aligned} \quad (31)$$

where

$$\begin{aligned}\gamma_s^*(r, \varphi) &= \gamma_s(r, \varphi) & \varphi_{L_k} \leq \varphi \leq \varphi_k \\ &= \gamma_s(r, \varphi) + \frac{d\Gamma(r)}{dr} & \varphi > \varphi_k\end{aligned}\quad (32)$$

The induced velocity due to a distribution of sources over the blade surfaces is given by

$$\vec{u}'_{\sigma}(x, r, \varphi) = - \sum_{k=1}^Z \frac{1}{4\pi} \int_{R_H}^R \sqrt{\lambda_i^2(\rho) + \rho^2} \int_{\varphi_{L_k}(\rho)}^{\varphi_{T_k}(\rho)} \sigma(\rho, \alpha) \nabla \frac{1}{|\vec{D}_s|} d\rho d\alpha \quad (33)$$

where $\sigma(r, \varphi)$ is the source strength density.

It follows that the lifting surface induced velocity may be considered as the sum of four terms

$$\begin{aligned}\vec{u}(x, r, \varphi) &= \underbrace{\vec{u}'_B(x, r, \varphi)}_{(1)} + \underbrace{\sum_{k=1}^Z \frac{1}{4\pi} \int_{R_H}^R \sqrt{\lambda_i^2(\rho) + \rho^2} \int_{\varphi_{L_k}(\rho)}^{\varphi_{T_k}(\rho)} \gamma_s^*(\rho, \alpha) \frac{\vec{e}_s \times \vec{D}_s}{|\vec{D}_s|^3}}_{(2)} \\ &\quad + \underbrace{[\vec{u}'_T(x, r, \varphi)]_{\text{lifting line}}}_{(3)} + \underbrace{\vec{u}'_{\sigma}(x, r, \varphi)}_{(4)}\end{aligned}\quad (34)$$

where

- ① = velocity due to a distribution of bound vorticity on the blade surface (equation (28))
- ② = velocity due to a distribution of free vorticity on the blade surface
- ③ = velocity due to the lifting line free-vortex sheet (equation (12))

④ = velocity due to a distribution of sources

In the method of Kerwin¹⁵ (available as a FORTRAN computer program FPV), the numerical evaluation is again based on discrete singularities. On the blade surface, a grid of radial and helical lines is constructed to form a lattice of source and vortex elements as illustrated in Figure 4. The elemental singularity strengths are determined as follows:

1. Radial vortex elements are required to produce the desired chord-wise load distribution and the known bound circulation $\Gamma(r)$ at each radius.
2. Helical vortex elements must satisfy conservation of vorticity.
3. Source and sink elements are required to generate the same chord-wise velocity distributions as the section thickness form would produce in two-dimensional flow. Also the sum of sources and sinks must equal zero.

As in the lifting-line analysis, the velocity is computed at a set of angular positions for each field point (x,r) and resolved into blade frequency harmonics.

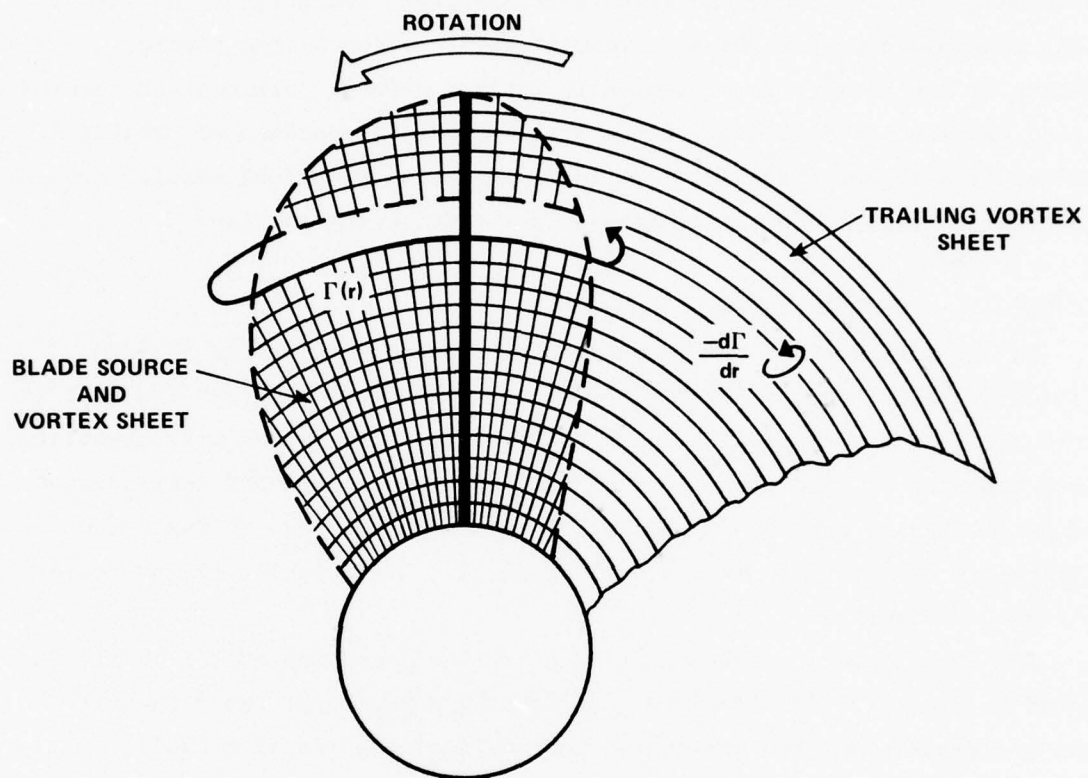
It may be noted that radial vortex lines (bound circulation) do not contribute to the steady axial and radial velocities and need only be computed to determine the strength of the helical (free) vortices on the blade. It is also straightforward to show that the steady velocity is

independent of the skew angle, $\frac{\varphi_{L_k} + \varphi_{T_k}}{2}$, as would be expected physically.

On the other hand, blade rake, the axial displacement of blade sections aft of the lifting line plane, is of marked importance. This is manifested in the free vorticity term (2) in equation (34) which "corrects" for the starting position of the trailing-vortex sheets. These and other features of the propeller calculations are best illustrated by considering specific examples.

EXAMPLE CALCULATIONS AND COMPARISON WITH EXPERIMENTS

The equations derived in the foregoing theoretical analyses have been programmed for computer-aided numerical solution. The calculation is performed by interfacing three separate programs: (1) the hull potential flow solution (PF), (2) propeller field point velocities (FPV), and (3) the



SOURCE AND VORTEX LINE MODEL OF PROPELLER BLADE

Figure 4 - Representation of Propeller Blade By Source and Vortex Line Lines (Projected View Looking Forward)

interaction analysis (CALCTD). A block diagram illustrating this procedure is given in Figure 5. It should be noted that the first, and most time-consuming task, is to assemble the necessary hull offsets and propeller geometry and loading data in a suitable form.

Example calculations have been conducted for several propeller body-of-revolution configurations, with and without cruciform stern appendages. These examples were chosen to illustrate important features of the analytical method and to provide experimental verification of the theory. A summary of the results is presented in Table 1 showing pertinent characteristics of each propeller-hull configuration and a comparison of predicted and measured thrust deduction fractions. Detailed numerical results and discussions of each example are given in the following sections.

EXAMPLE 1: APPENDED SERIES 58 FORM

As a first check on the computational procedure, a Series 58 Form originally calculated by Beveridge⁶ was selected for analysis. The hull is a streamlined body of revolution, DTNSRDC Model 4620, fitted with cruciform stern appendages. The propeller, DTNSRDC 3638, is a 5-bladed wake-adapted design located 98 percent of the hull length from the bow. Offsets and particulars of the hull are listed in Table 2. A drawing of the propeller is given in Figure 6.

The quadrilateral representation of the hull and appendages is illustrated in Figure 7 (identical to that used by Beveridge). Note that for ease of computation, the horizontal control surfaces are also used to represent the upper and lower rudders and the forebody is approximated by reflecting the afterbody about the hull midlength (this latter simplification is shown to be valid in later examples). The propeller circulation and hydrodynamic pitch distributions, $\Gamma(r)$ and $2\pi r \tan \beta_1(r)$, were obtained from lifting-line calculations and are shown in Figure 8. The axial and radial propeller field point velocities induced at control points on the body boundary are presented in Figure 9. Since the propeller has no rake, the lifting-surface corrections arise solely from blade thickness and chordwise load distribution. These effects are seen to decay more rapidly than the lifting-line disturbance field, contributing less than 10 percent at distances beyond one propeller radius.

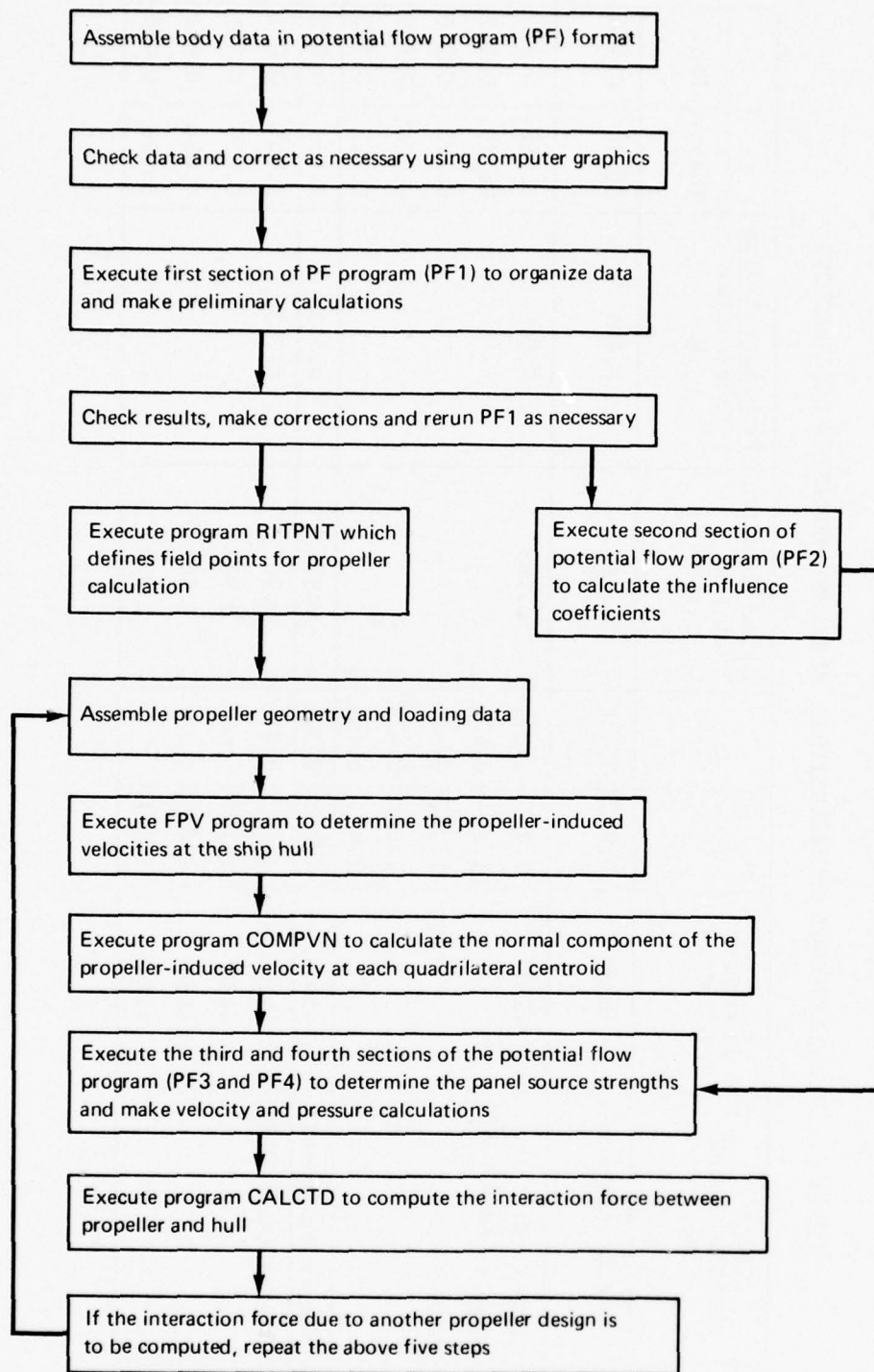


Figure 5 - Interaction Analysis - Computational Procedure

TABLE 1 - PROPELLER-BODY CONFIGURATIONS IN THRUST DEDUCTION CALCULATIONS

Example	Body (DTNSRDC Model) No.	Propeller (DTNSRDC No.)	J _V	C _{Th}	Axial Location of Prop ξ (x/L)	$\frac{\text{Propeller Radius}}{\text{Body Radius}}$ $\frac{R}{R_B}$	t	
							Theory	Exp.
1.	4620 (Appended)	3638	0.972	0.480	0.980	0.404	0.135	0.150
2.	5225-1 (No 5225-2 Appendages) 5225-3	4577	1.25	0.371	0.983	0.545	0.068	0.070
			1.25	0.420			0.129	0.143
			1.07	0.637			0.126	0.140
			1.25	0.428			0.106	0.109
			1.07	0.646			0.103	0.103
3.	5224-1 (Appended)	4567A	1.250	0.370	0.984	0.545	0.091	0.075
4.	5224-2 (Appended)	4486	1.490	0.210	0.965	0.743	0.051	0.091
		4487	1.500		0.964		0.059	0.109
		4488	1.471		0.961		0.034	0.064
		4489	1.471		0.970		0.026	0.036

TABLE 2 - OFFSETS AND PARTICULARS FOR SERIES 58 FORM, MODEL 4620^{6,23}

x	X in.	y	Y in.	x	X in.	y	Y in.
0.00	000.0	0.0000	0.000	0.52	93.6	0.4818	11.82
0.02	3.6	0.1427	3.500	0.54	97.2	0.4755	11.66
0.04	7.2	0.2029	4.977	0.56	100.8	0.4684	11.49
0.06	10.8	0.2490	6.108	0.58	104.4	0.4603	11.29
0.08	14.4	0.2873	7.047	0.60	108.0	0.4513	11.07
0.10	18.0	0.3200	7.850	0.62	111.6	0.4414	10.83
0.12	21.6	0.3485	8.549	0.64	115.2	0.4305	10.56
0.14	25.2	0.3734	9.160	0.66	118.8	0.4187	10.27
0.16	28.8	0.3953	9.697	0.68	122.4	0.4058	9.954
0.18	32.4	0.4145	10.17	0.70	126.0	0.3919	9.613
0.20	36.0	0.4312	10.58	0.72	129.6	0.3768	9.243
0.22	39.6	0.4457	10.93	0.74	133.2	0.3605	8.843
0.24	43.2	0.4581	11.24	0.76	136.8	0.3429	8.411
0.26	46.8	0.4687	11.50	0.78	140.4	0.3239	7.945
0.28	50.4	0.4775	11.71	0.80	144.0	0.3036	7.447
0.30	54.0	0.4848	11.89	0.82	147.6	0.2817	6.910
0.32	57.6	0.4905	12.13	0.84	151.2	0.2582	6.334
0.34	61.2	0.4947	12.12	0.86	154.8	0.2330	5.715
0.36	64.8	0.4977	12.21	0.88	158.4	0.2060	5.053
0.38	68.4	0.4994	12.25	0.90	162.0	0.1771	4.344
0.40	72.0	0.5000	12.27	0.92	165.6	0.1461	3.584
0.42	75.6	0.4995	12.25	0.94	169.2	0.1131	2.774
0.44	79.2	0.4979	12.21	0.96	172.8	0.0778	1.908
0.46	82.8	0.4953	12.15	0.98	176.4	0.0401	0.984
0.48	86.4	0.4917	12.06	1.00	180.0	0.0000	0.000
0.50	90.0	0.4878	11.97				
Model 4620				Wetted Surf. Coeff. = .7324			
Serial 40050060-73				LCB, x = 0.4456			
Formula:				L/D = 7.339			
$y^2 = a_1x + a_2x^2 + a_3x^3 + a_4x^4 + a_5x^5 + a_6x^6$				Model Particulars:			
where: $a_1 = 1.000000$				Length, ft = 15.0000'			
$a_2 = + 1.137153$				Diameter, ft = 2.044 (24.53 in)			
$a_3 = -10.774885$				Nose radius, ft = 0.1392 (1.670 in)			
$a_4 = +19.784286$				Tail radius, ft = 0.0000			
$a_5 = -16.792534$				Wetted Surf., ft ² = 70.55			
$a_6 = + 5.645977$				Volume, ft ³ = 29.53			
				LCB, ft = 6.6840			

²³Landweber, L. and M. Gertler, "Mathematical Formulation of Bodies of Revolution," DTMB Report 719 (Sept 1950).

DIA. MODEL IN'S.	PITCH MODEL IN'S.	PITCH RATIO	MEAN WIDTH RATIO	NO. OF BLADES	TOTAL PROJ. AREA	RAKE ANGLE	P.A. D.A.	EXP. A D.A.	B.T.F.	DIRECTION OF ROTATION
9.900	9.415	0.951	0.242	5	41.950	—	0.545	0.611	VAR.	R.H.

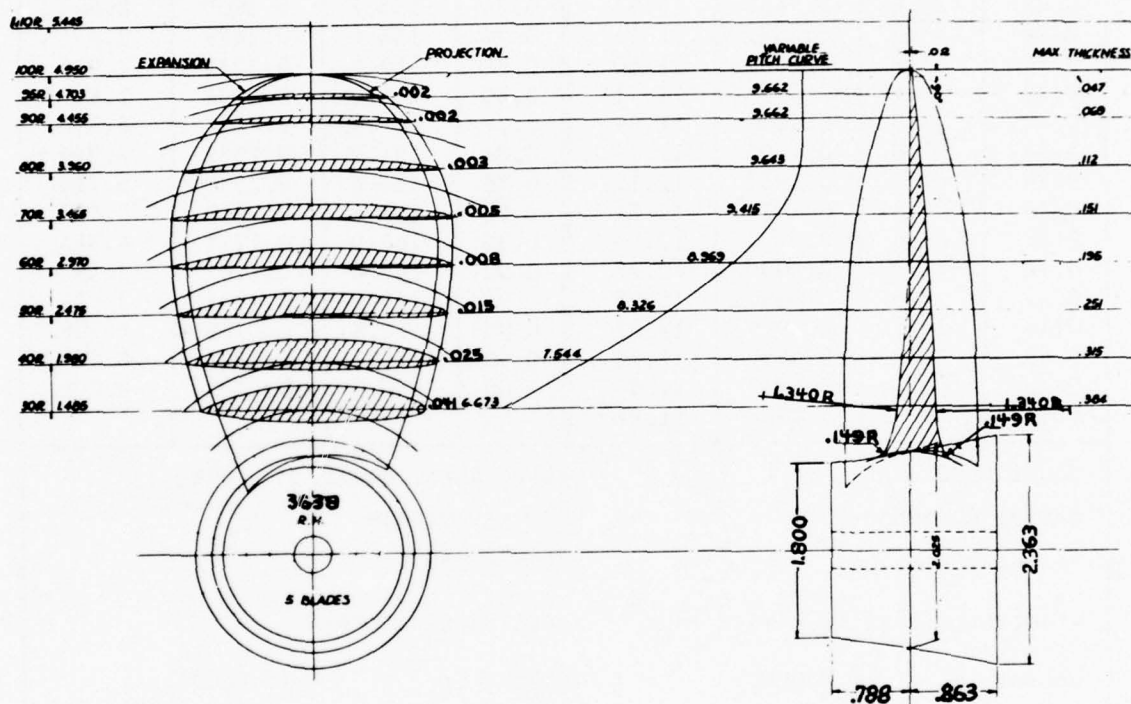


Figure 6 - Propeller 3638

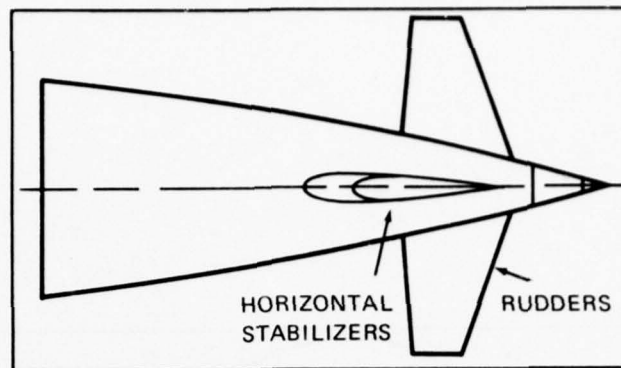


Figure 7a - Stern Appendage Configuration - NSRDC Model 4620

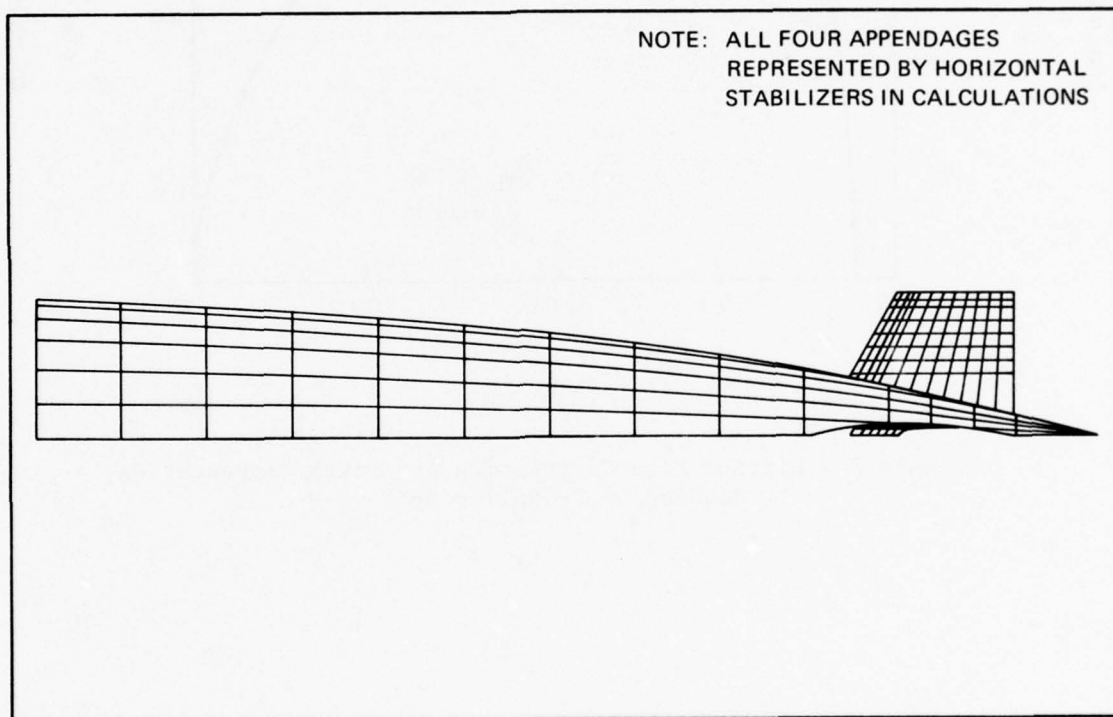


Figure 7b - Quadrilateral Representation of NSRDC Model 4620

Figure 7 - Representation of NSRDC Model 4620

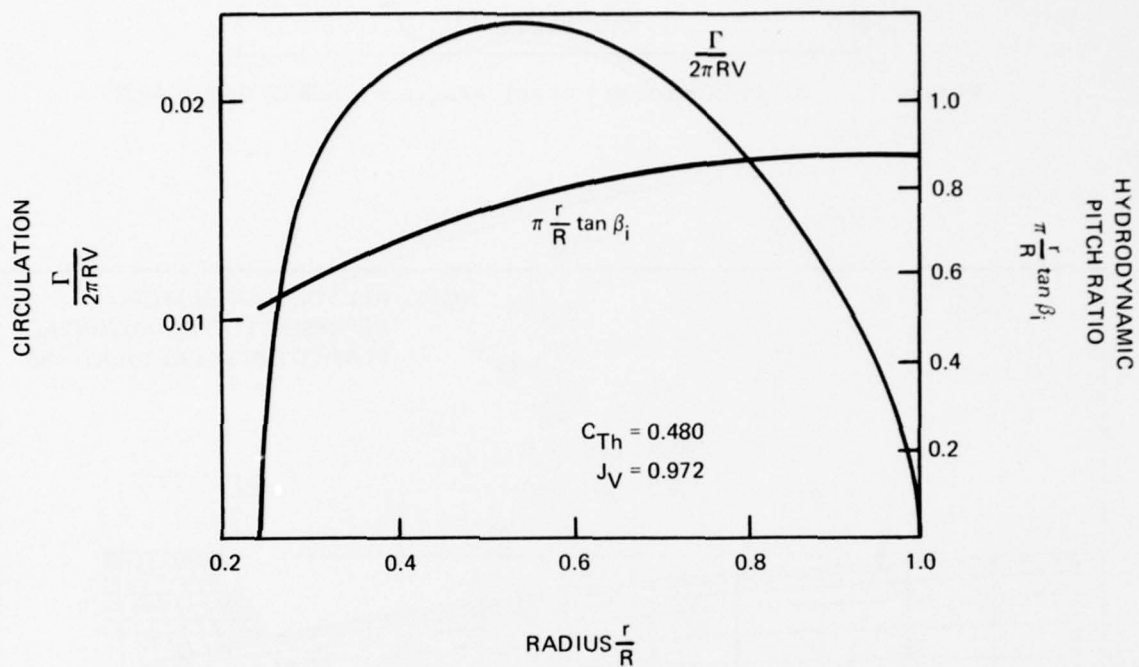


Figure 8 - Lifting Line Circulation and Pitch Representing Loading of Propeller 3638

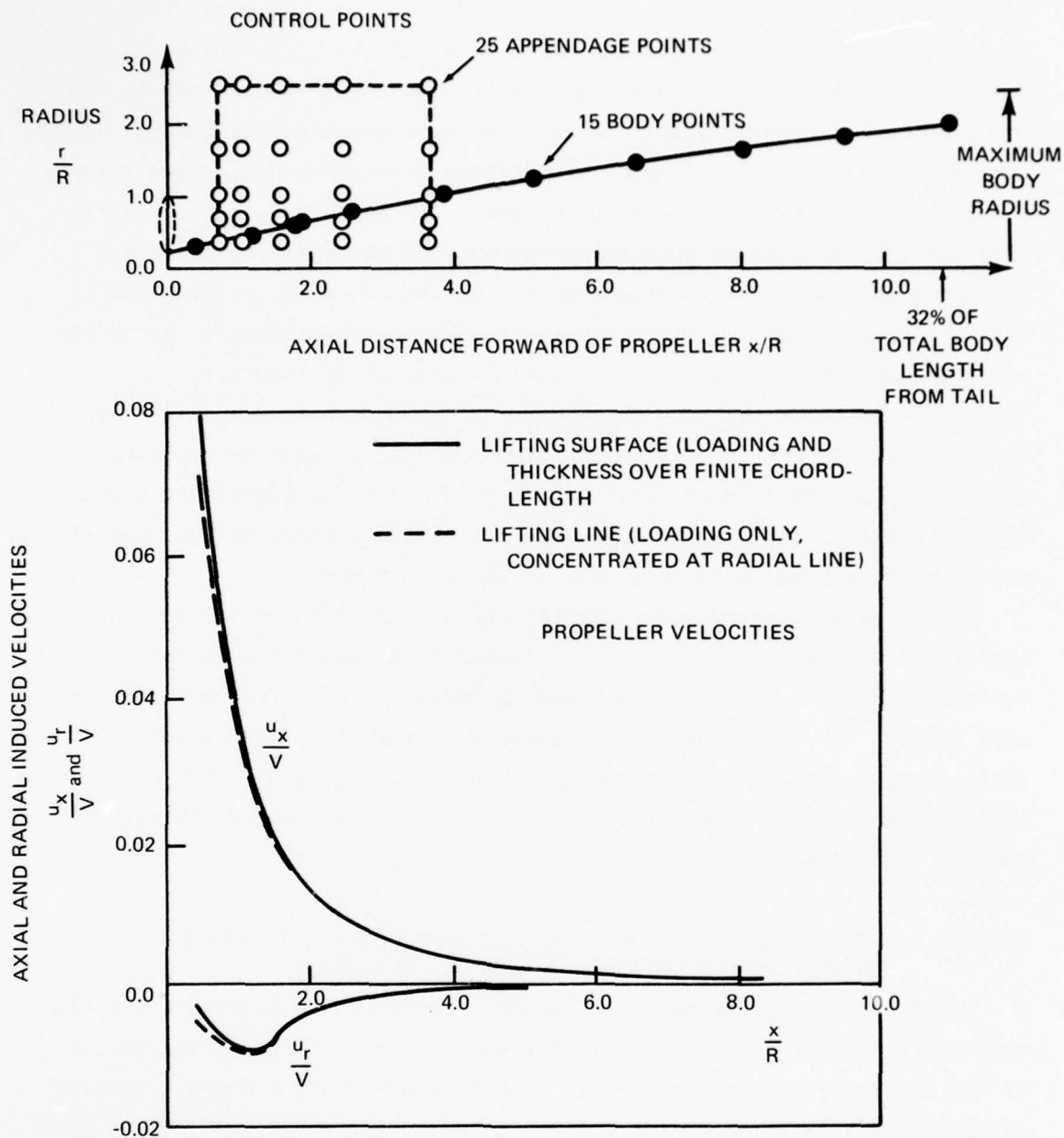


Figure 9 - Control Points and Propeller Induced Velocities on Appended Series 58 Body

The computed values of thrust deduction and the measured result obtained from model resistance and self-propulsion experiments are shown in Table 3. Since no correction for increased frictional drag has been included, the potential flow prediction of $(1-t)$ should be higher than the measured value*. The agreement between the two calculated values (pressure integration and Lagally theorem) indicates good numerical accuracy. Also note that the correction to body singularity strengths changes the thrust deduction fraction by less than 3 percent. The comparison between lifting-line and lifting-surface predictions shows that the influence of blade thickness and chordwise loading reduces the thrust deduction fraction by only 4 percent. The agreement between theory and experiment is quite encouraging and is considered to be within experimental accuracy.

It is believed that the discrepancy between Beveridge's result and the current work lies in the derivation of the propeller sink-disk strength. Beveridge used the induced axial velocity *at a lifting line*. The present method (equation 27) properly averages the velocity field at the disk plane, resulting in a lower sink strength, as shown in Figure 10.

It is also of interest to examine the distribution of the interaction force over the afterbody. This is a function of both the body sectional-area distribution and the breadth and intensity of the propeller disturbance field. The longitudinal distribution of the thrust deduction, $(dt(x)/dx)$, acting on the *body only*, is shown in Figure 11. The significant contribution is over the last 25 percent of the body length with 50 percent concentrated in the last 6 percent of the length.

EXAMPLE 2: COMPARISON OF THEORETICAL AND EXPERIMENTAL PRESSURE DISTRIBUTIONS ON THREE BODIES OF REVOLUTION

Wind-tunnel experiments were recently conducted to determine the flow characteristics of three streamlined bodies of revolution.⁹ Measurements of the afterbody pressure distribution with and without a stern propeller in operation were obtained for comparison with analytical predictions. The profile of the parent body (DTNSRDC Model 5225-1) is shown in Figure 12

*The added frictional resistance is expected to increase the value of t by no more than 5 percent, based on Reference 9.

TABLE 3 - COMPUTED* AND MEASURED VALUES OF THRUST DEDUCTION FRACTION FOR
APPENDED SERIES 58 BODY (DTNSRDC MODEL 4620, PROPELLER 3638)

METHOD		1-t
Measured (Resistance and Self-Propulsion Experiment)		0.850
Computed	Lifting Surface Method	0.865
	Body Pressure Integration (Equation (11))	0.864
	Lagally Theorem (Equation (13))	0.867
	Lagally Theorem (without Corrections, to Body Source Strengths)	0.859
	Lagally Theorem (Equation (13))	0.841
Lifting Line (Sink-Disk) Method		
Lagally Theorem Applied to Propeller Sink-Disk Without Corrections to Body Source Strengths (Beveridge 6)		

*Without Corrections for Increased Frictional Resistance

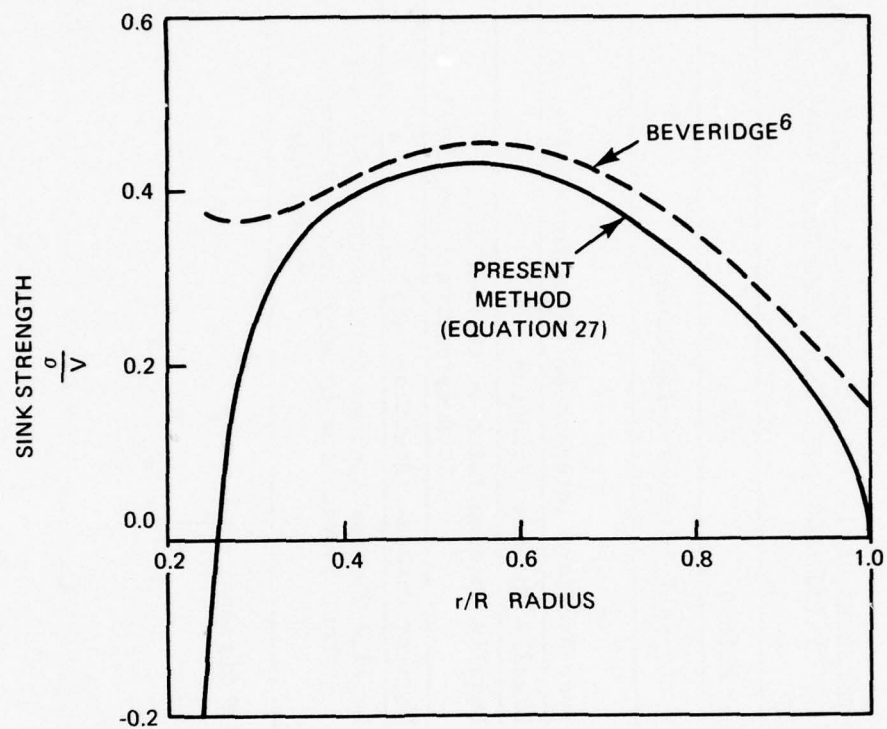
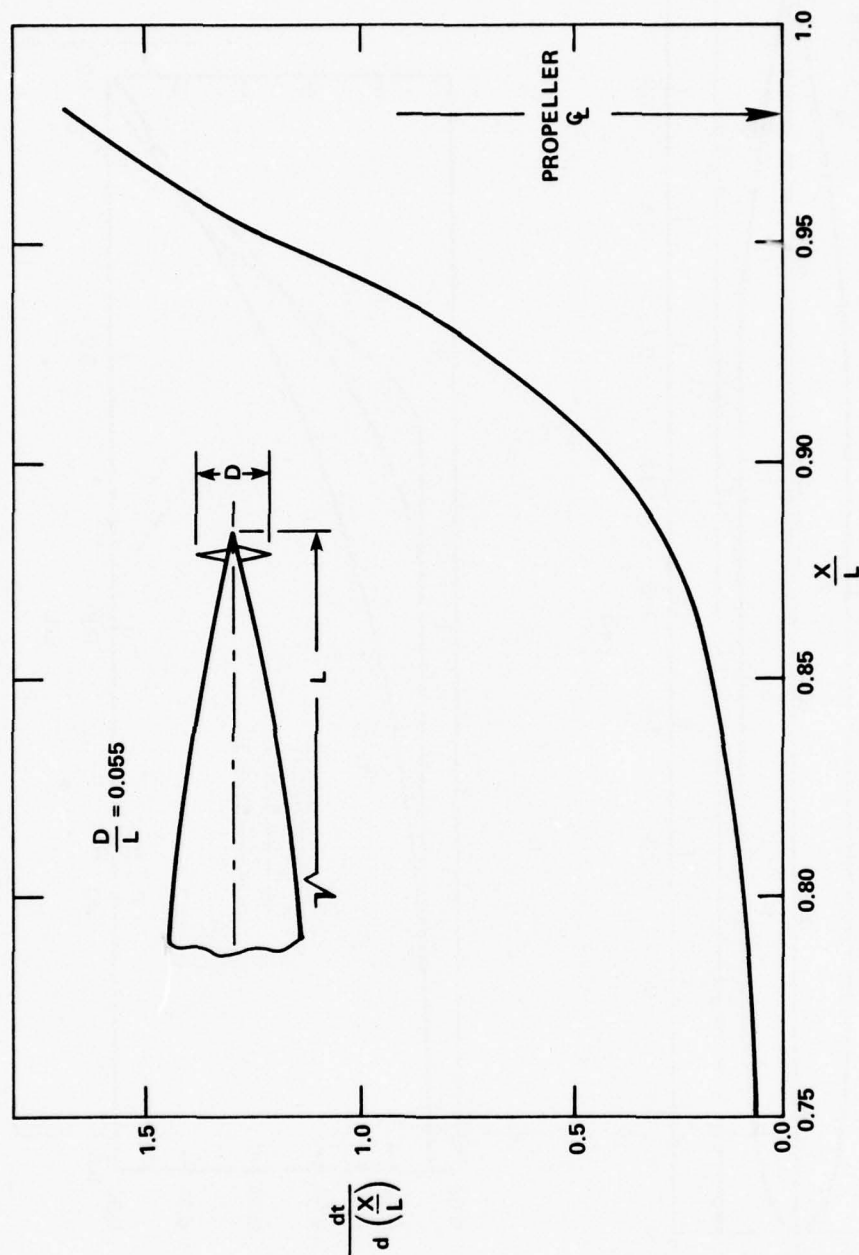


Figure 10 - Radial Distribution of Propeller Sink Strength
Derived From Lifting Line Calculations



CALCULATED LONGITUDINAL DISTRIBUTION OF THRUST DEDUCTION MODEL 4620

Figure 11 - Calculated Longitudinal Distribution of Thrust Deduction Force on Model 4620 (Body Only)

Figure 12 - Representation of DTNSRDC Models 5225-1, 5225-2, and 5225-3

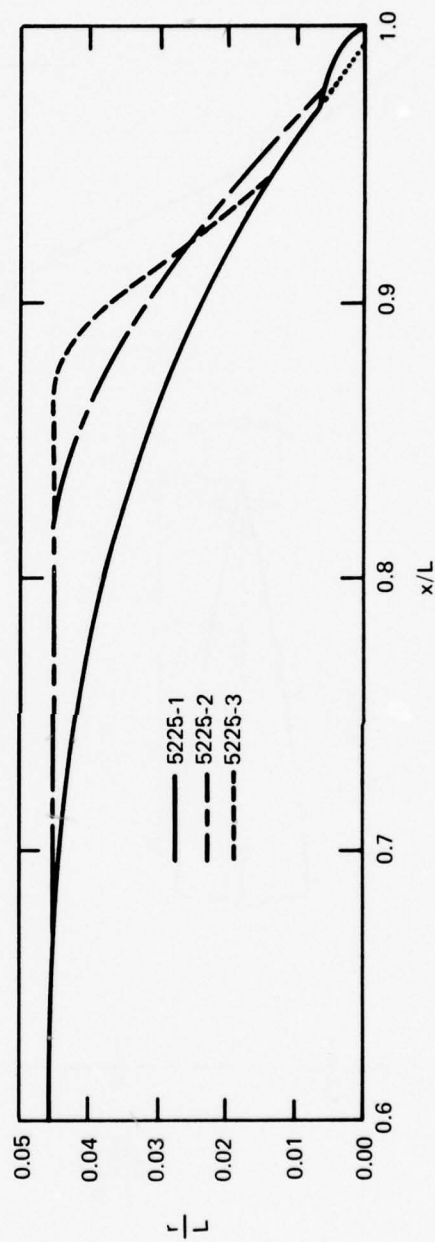
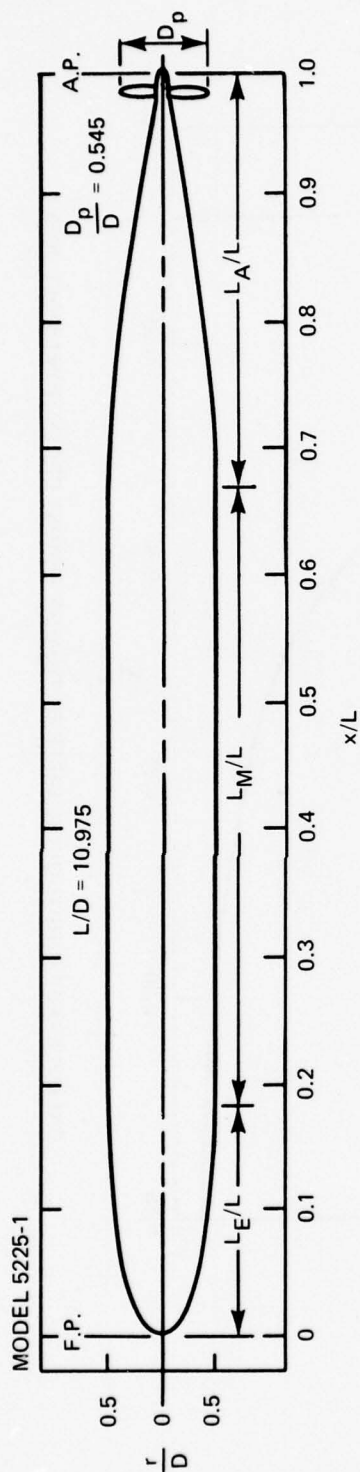


Figure 12a - Profiles of Axisymmetric Afterbodies

Figure 12 (Continued)

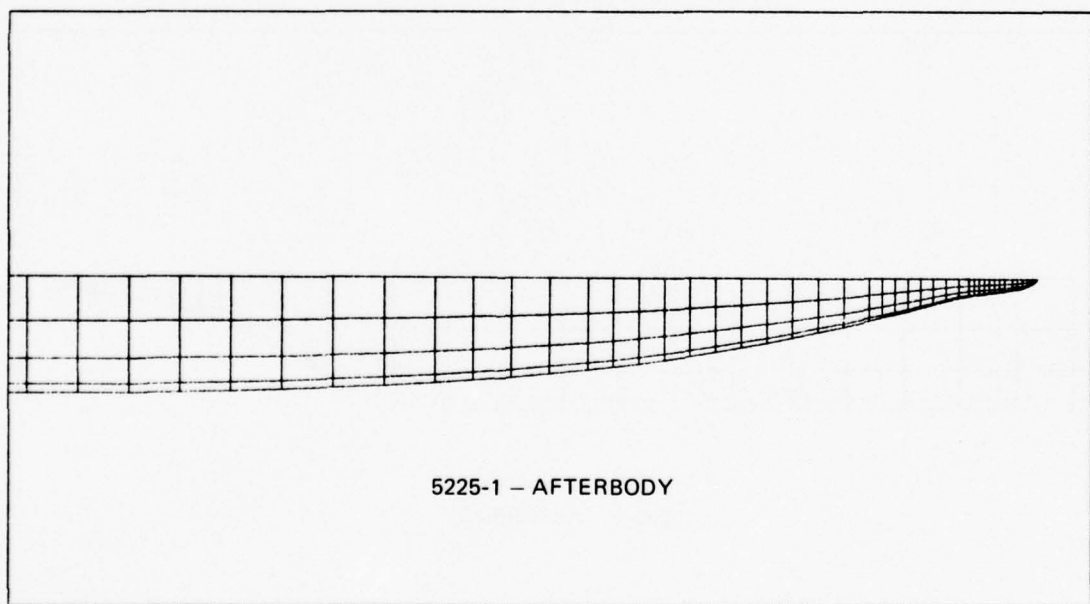
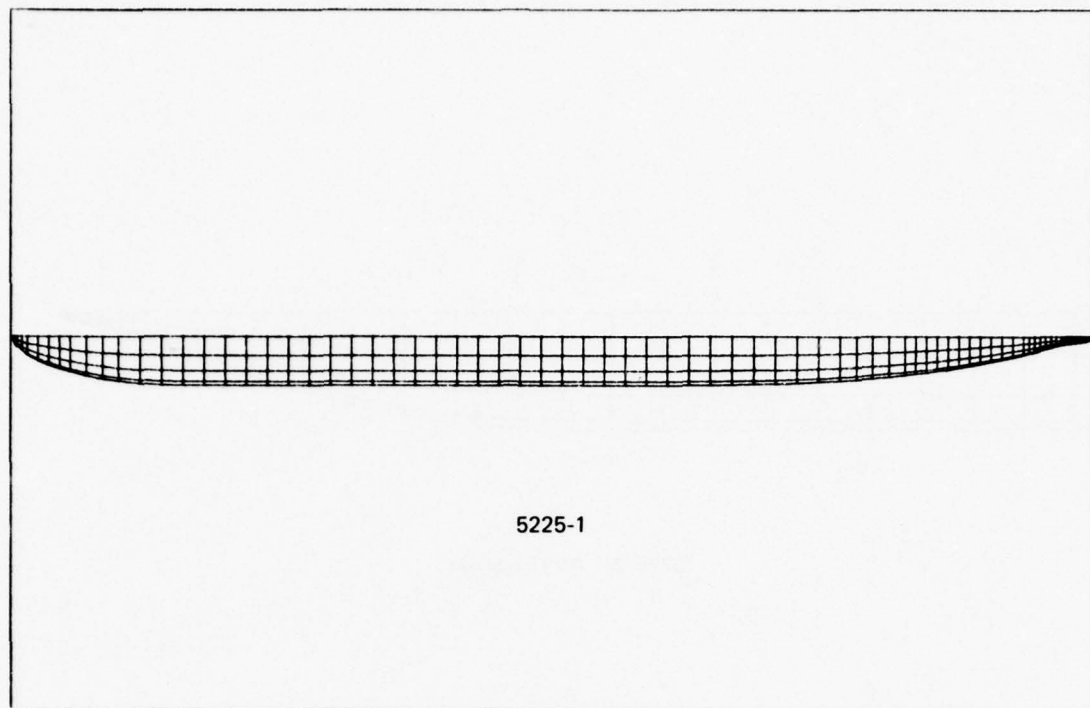


Figure 12b - Quadrilateral Representation of Bodies of Revolution,
DTNSRDC Models 5225-1, 5225-2, and 5225-3

Figure 12 (Continued)

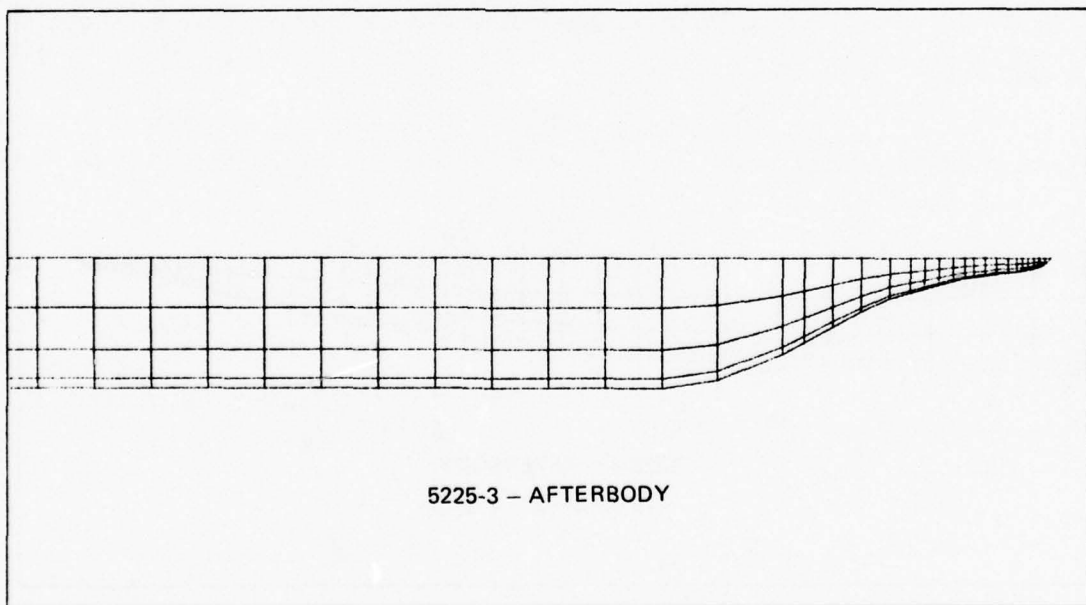
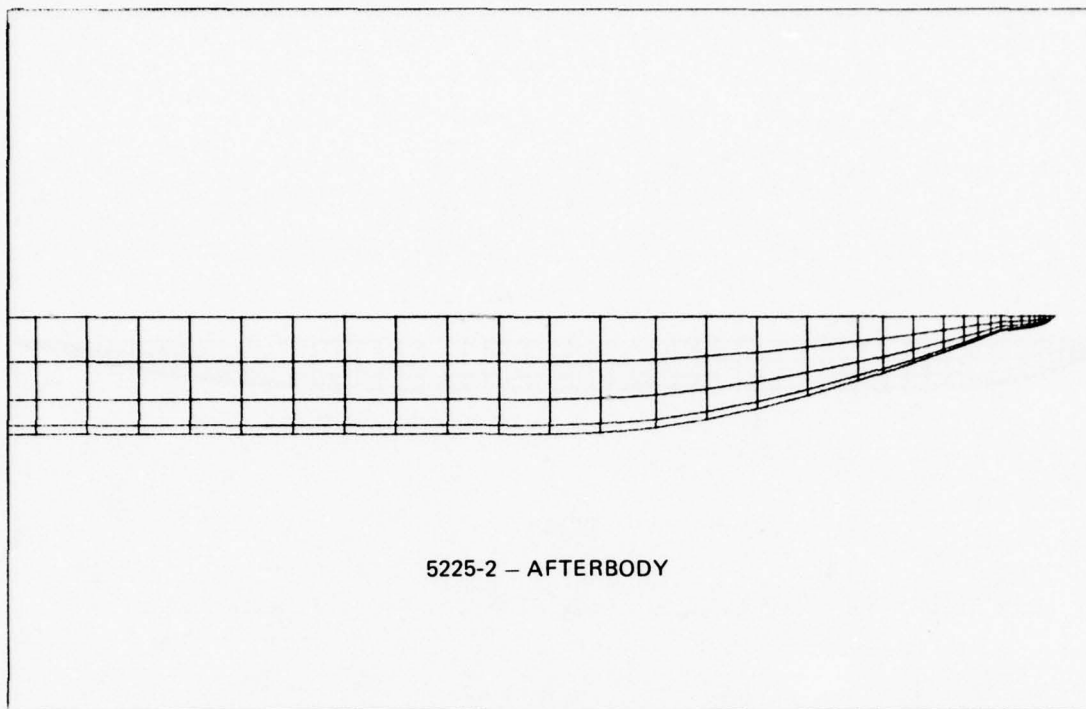


Figure 12b (Continued)

along with the quadrilateral representation used in the calculations. The other two bodies, DTNSRDC Models 5225-2 and 5225-3, differ from the parent in afterbody shape only and are also illustrated in Figure 12.

One 7-bladed propeller model, DTNSRDC Model 4577, was used for the three body experiments. The principal characteristics and geometry of the propeller are summarized in Table 4. Pressure measurements were obtained at two advance ratios, $J = 1.25$ and $J = 1.07$. Since the propeller was not operating in its design wake, it was necessary to predict the load distribution using an inverse performance calculation.²¹ This was an iterative process, starting with the measured nominal wake, computing a load distribution, recomputing the wake, and so on. Convergence was achieved after two iterations.

The computed and measured differences in afterbody pressure distribution are shown in Figures 13a, 13b, and 13c. The agreement is excellent for body 5225-1 and very good for body 5225-2. There is a marked discrepancy for 5225-3. This body was intentionally designed to have boundary layer separation in the absence of the propeller with the hope that the propeller influence would reattach the flow. However, flow separation occurred at $x/L = 0.92$ which is too far upstream. The thrust deduction fraction, t_{exp} , was derived by integrating the measured pressure difference and dividing by the calculated propeller thrust (no self-propulsion experiments were conducted). The results are compared in Figure 13 with the theoretically computed values, t_{calc} . The agreement for body 5225-3 is considered fortuitous in view of the difference in pressure distribution. The thrust deduction for body 5225-2 is larger than for 5225-1 which is expected on physical grounds since the fuller afterbody places the frontal area closer to the propeller. Body 5225-3, which has the fullest afterbody, is actually finer in the immediate vicinity of the propeller; hence, the calculated thrust deduction is also lower than for body 5225-2.

TABLE 4 - GEOMETRY OF PROPELLER 4577

Number of Blades			7	
Expanded Area Ratio			0.584	
Section Meanline			NACA a = 0.8	
Section Thickness Distribution			BUSHIPS Type II ²⁴	
rake Angle, deg			6.964	
Skew, deg			30	
r/R	C/D	t/C	P/D	f_M/C
0.2106	0.171	0.235	0.823	0.0014
0.3	0.177	0.209	0.980	0.0175
0.4	0.182	0.182	0.151	0.0288
0.5	0.185	0.158	0.243	0.0337
0.6	0.185	0.135	1.264	0.0341
0.7	0.180	0.116	1.248	0.0311
0.8	0.164	0.0995	1.206	0.0246
0.9	0.132	0.0875	1.157	0.0141
1.00	0.069	0.0813	1.108	0.

²⁴ Brockett, T., "Minimum Pressure Envelopes for Modified NACA-66 Sections with NACA a = .8 Camber and BUSHIPS Type I and II Sections," DTNSRDC Report 1780 (Feb 1966).

Figure 13 - Measured and Calculated Pressure Distributions on DTNSRDC Models 5225-1, 5225-2, and 5225-3

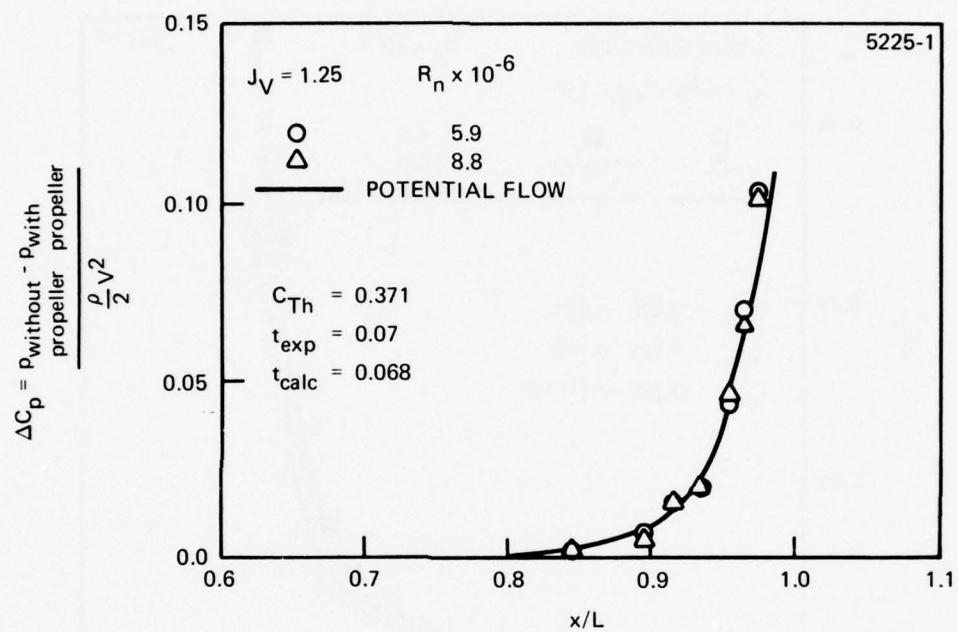


Figure 13a - Body 5225-1

Figure 13 (Continued)

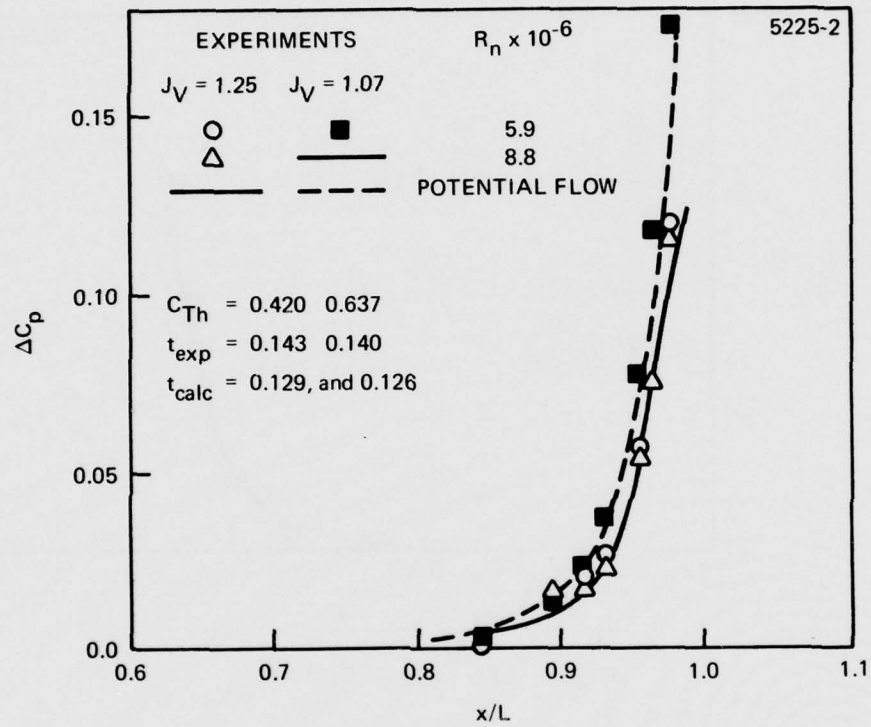


Figure 13b - Body 5225-2

Figure 13 (Continued)

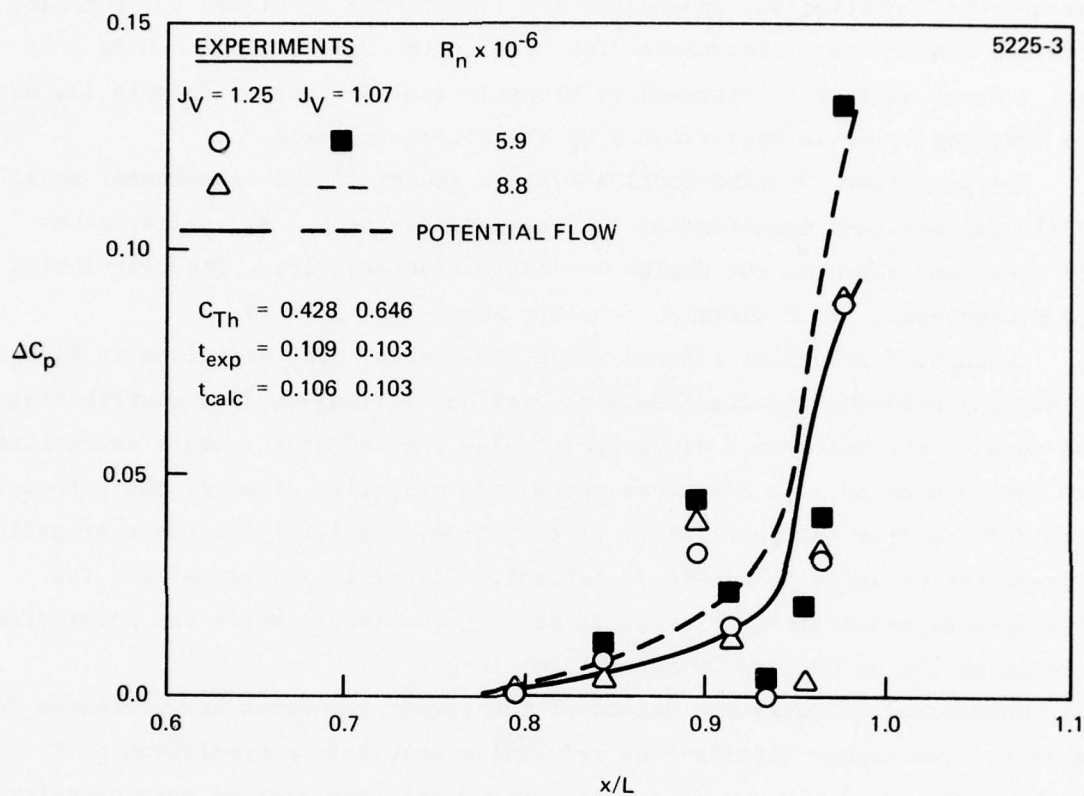


Figure 13c - Body 5225-3

EXAMPLE 3: BODY OF REVOLUTION WITH STERN APPENDAGES

This example provides a further comparison of computed and measured thrust deduction and exhibits the separate contribution of stern appendages. The analysis is applied to an appended body of revolution, represented by DTNSRDC Model 5224-1. This model, with appendages removed, is a geosym of the wind-tunnel model, DTNSRDC 5225-1, described previously in Example 2. The afterbody profile and appendages are illustrated in Figure 14, together with the quadrilateral representation used in the calculations. Note that each control surface is represented properly (in contrast to Example 1), but the forebody is again approximated by the afterbody image.

The propeller, DTNSRDC Model 4567A, (a geosym of the wind-tunnel model 4577), was designed specifically for the appended body. All calculations are therefore based on the design loading characteristics. The circulation and hydrodynamic pitch distributions are shown in Figure 15.

Calculated propeller induced velocities on the body are given in Figure 16 showing both the lifting-line sink disk and lifting-surface contributions. The results derived from a simple point sink located at the shaft centerline are also presented. At distances beyond one propeller diameter the velocities derived from the point sink, lifting-line, and lifting-surface propeller representation agree to within 10 percent. Closer to the propeller, the lifting-line velocities are about 25 percent too large, while the point-sink velocities are as much as 50 percent too large.

Calculated and measured values of the thrust deduction are presented in Table 5. The higher lifting-line velocities result in a prediction of t which is 21 percent larger than that derived from the lifting surface calculation. The predicted value of $(1-t)$, while lower than the measured value, is within experimental accuracy. The contribution of the stern appendages, as shown in Table 5, is 24 percent of the total thrust deduction. (Although not discussed in Example 1, a comparable value of 25 percent is found in that case). Finally, the distribution of interaction force on the afterbody is displayed in Figure 17, shown as the integrated force as a function of distance from the stern. The significant contribution is over the last 30 percent of the body length with 50 percent of the force concentrated in the last 5 percent (i.e., within a distance of one propeller diameter).

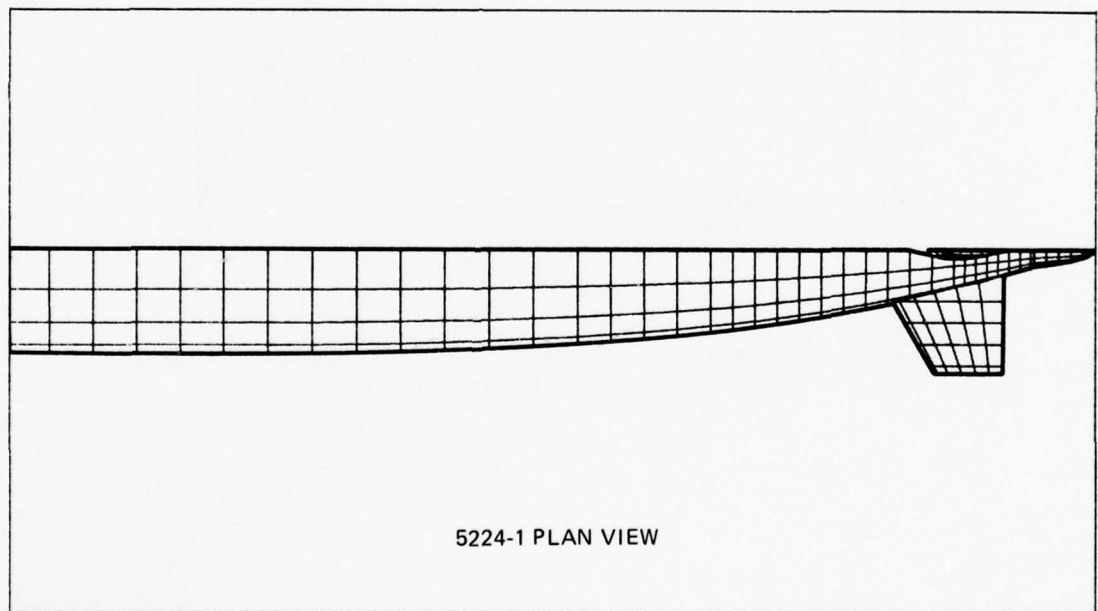
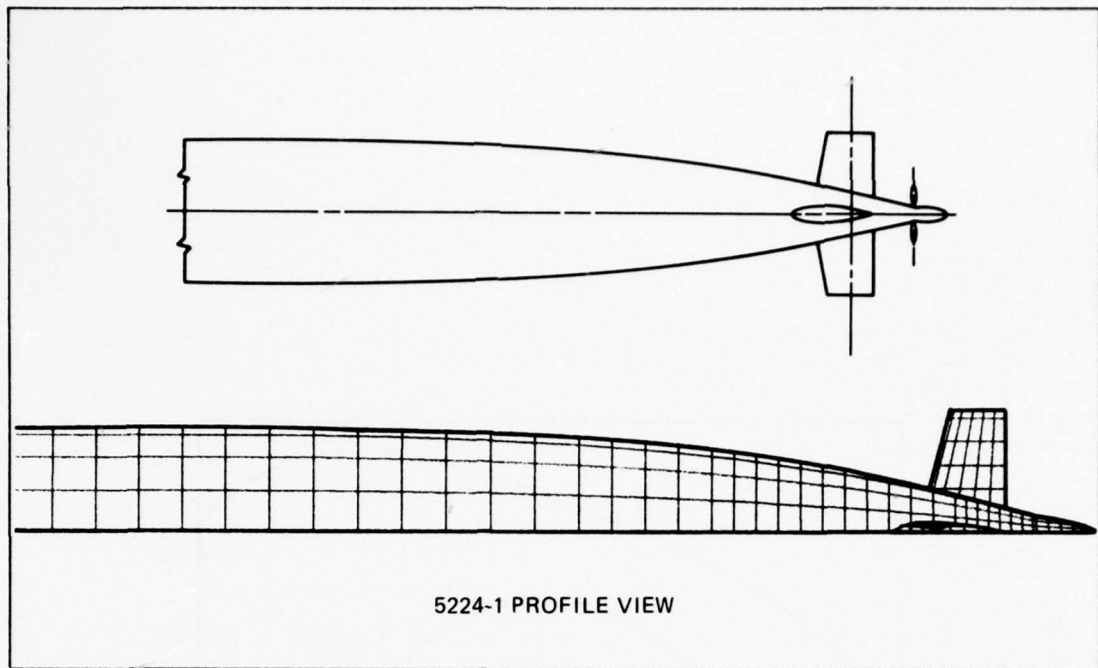


Figure 14 - Profile and Quadrilateral Representation of
DTNSRDC Model 5224-1

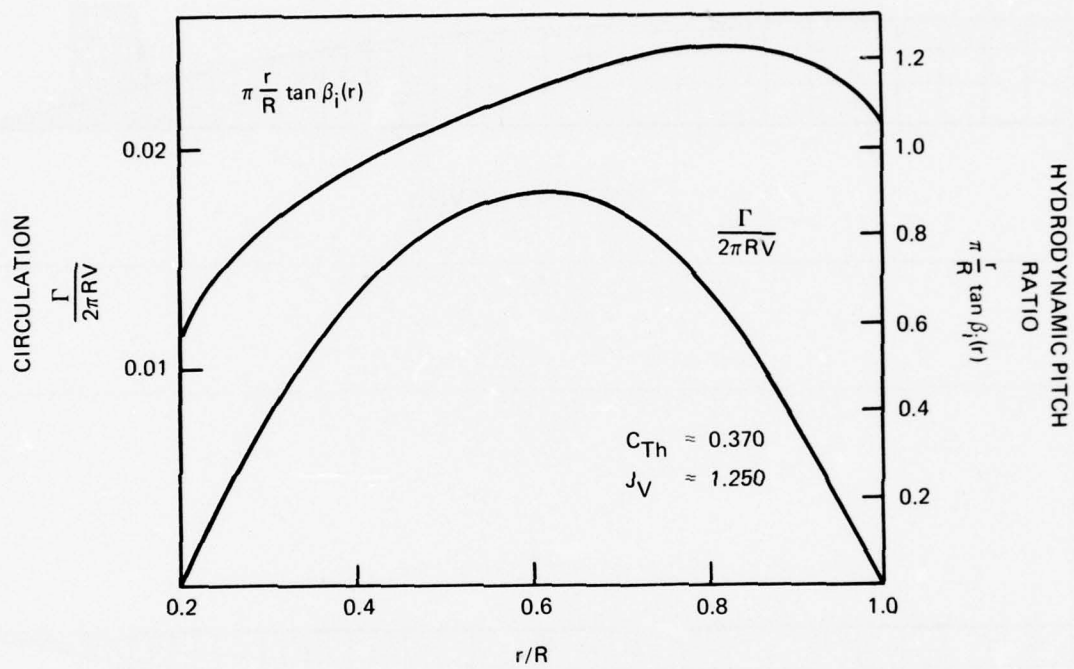


Figure 15 - Design Circulation and Hydrodynamic Pitch Distributions of Propeller 4567A

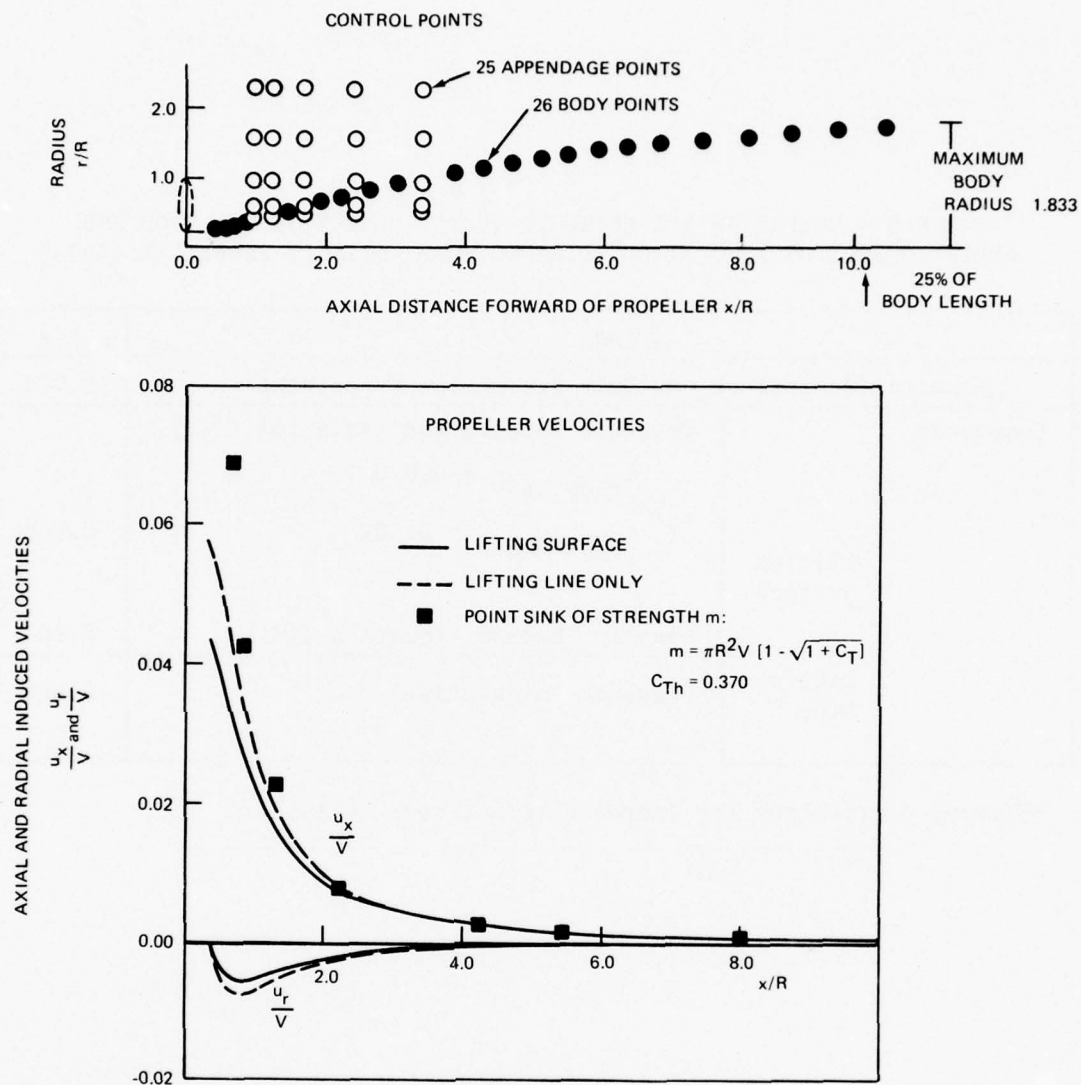


Figure 16 - Control Points and Propeller Induced Velocities
on Appended Body of Revolution (DTNSRDC 5224-1)
Propeller 4567A

TABLE 5 - COMPUTED* AND MEASURED THRUST DEDUCTION FRACTION FOR
APPENDED BODY OF REVOLUTION (DTNSRDC MODEL 5224-1, PROPELLER 4567A)

METHOD			1-t
Measured (Resistance and Self Propulsion Experiment)			0.925
Computed*	Lifting Surface	Pressure Integration (Equation (11))	0.908
		$t_{\text{Body Only}} = 0.070$	
		$t_{\text{Appendages}} = 0.022$	
	Lifting Line	Lagally Theorem (Equation (13))	0.904
		Pressure Integration	0.888

*Without Corrections for Increased Frictional Resistance

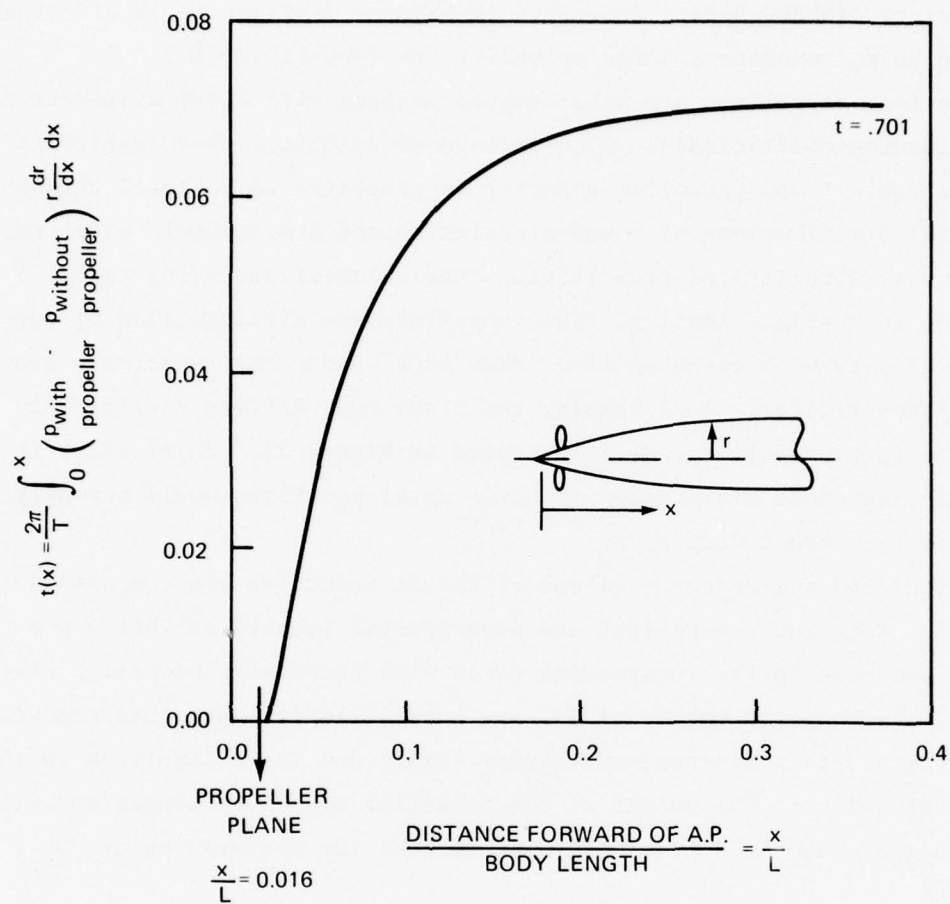


Figure 17 - Longitudinal Distribution of Thrust Deduction
 (Cumulative From Stern) on Body of Revolution
 (DTNSRDC Model 5224-1, Propeller 4567A)

EXAMPLE 4: APPENDED BODY OF REVOLUTION WITH FOUR RAKED PROPELLERS

In this example the thrust deduction analysis is applied to compare four different propellers fitted to the same hull. The hull is an appended body of revolution, represented by DTNSRDC Model 5224-2. This model is identical to DTNSRDC 5224-1 described in Example 3 except for a slight modification to accommodate a large propeller hub (see Figure 18).

The four propellers are wake-adapted designs with equal diameters and thrust loading coefficients. A comparison of principal characteristics is given in Table 6 and propeller geometry is presented in Tables 7 through 10. The radial distributions of bound circulation and hydrodynamic pitch shown in Figure 19 were derived from lifting-line calculations using Lerbs'¹⁸ criterion for optimum loading. The propellers are distinguished by varying amounts of skew with corresponding "skew back" along the respective geometric pitch helices. As a result, the blade *rake* differs considerably among the four propellers, as illustrated in Figure 20. Physically, it was expected that these differences in blade axial positions would strongly influence the thrust deduction.

Calculated and measured values of thrust deduction are compared in Table 11. Both the theoretical and experimental results exhibit a pronounced decrease in the interaction force with increasing propeller rake. However, the computed values of $1-t$ are substantially lower than measured in each case. This discrepancy is very likely due to difficulties in the experiment owing to the weight of the propeller models.* Comparison with the result of Example 3 provides evidence that the measured values of t are too high.

The calculated contributions of the stern appendages to the thrust deduction are given in Table 11. These vary from 19 to 24 percent of the total, which is comparable to the result of example 3. In Figure 20 the rake distribution of propeller 4567A is shown as a dashed line and may be compared with propeller 4487. Since propeller 4487 is further aft on the body and has a larger diameter, the thrust deduction fraction should be lower. This is, in fact, predicted from theory (0.059 versus 0.09), while the experiments yield a higher result for 4487 (0.109 versus 0.09).

*These models were approximately 5 times heavier than typical models due to material (bronze instead of aluminum) and size.

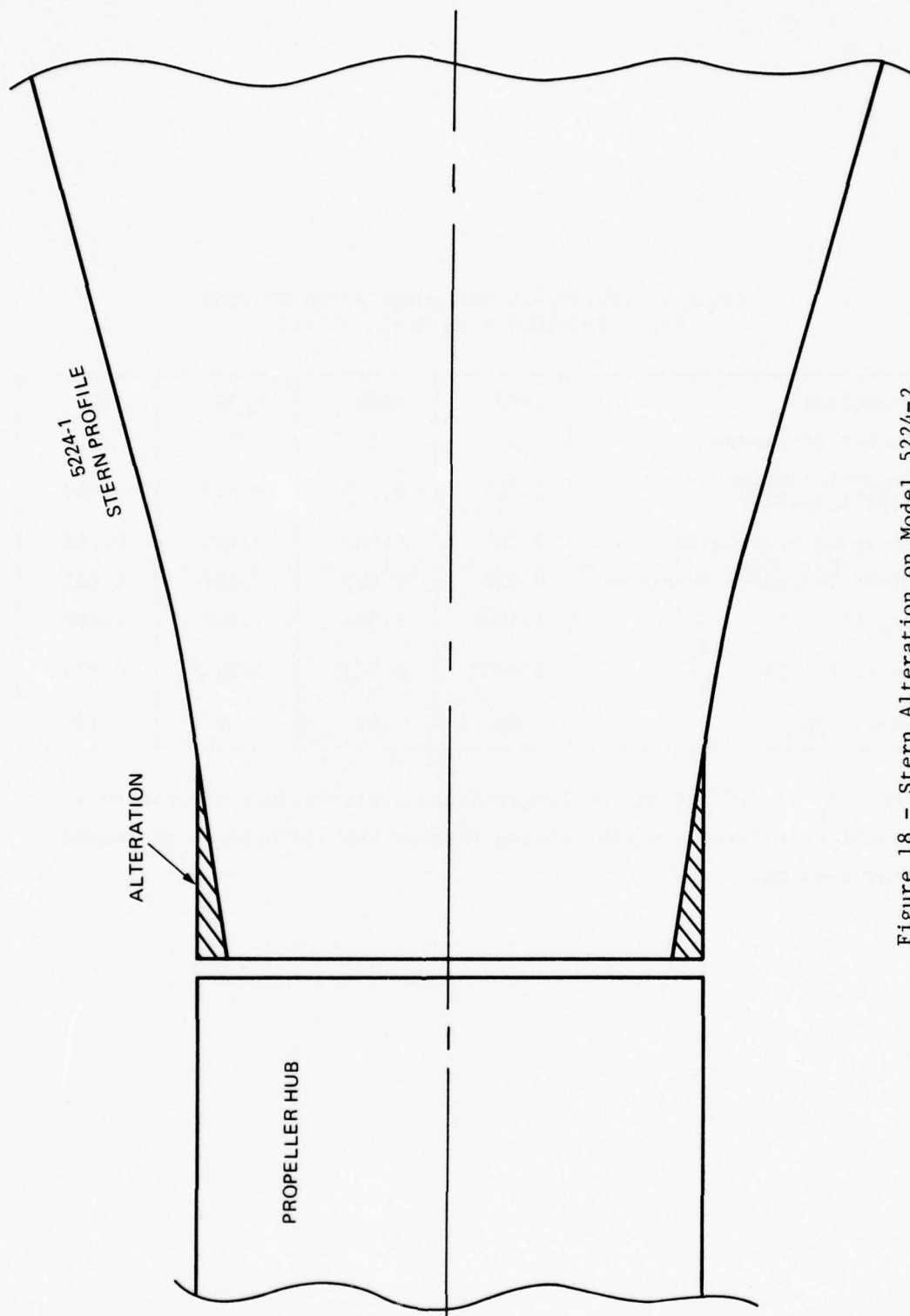


Figure 18 - Stern Alteration on Model 5224-2

TABLE 6 - PRINCIPAL CHARACTERISTICS OF FOUR
RAKED PROPELLERS ON MODEL 5224-2

Propeller	4487	4486	4488	4489
Number of Blades	7	5	3	3
$\frac{\text{Propeller Diameter}}{\text{Hull Diameter}}$	0.743	0.743	0.743	0.743
Expanded Area Ratio	0.707	0.707	0.707	0.709
Blade Thickness Fraction	0.036	0.047	0.077	0.083
P/D at 0.7R	1.4975	1.503	1.519	1.498
Axial Position, $\frac{X_p}{L}$	0.8637	0.9652	0.9678	0.9703
Skew, Deg	32	43	72	120

*Here X_p is defined as the longitudinal distance from the bow to a propeller reference plane passing through the midchord of the blade root section.

TABLE 7 - GEOMETRY OF PROPELLER 4486

Number of Blades 5

Expanded Area Ratio 0.707

Section Meanline NACA a = 0.8

Section Thickness Distribution NACA 66 (DTNSRDC modified nose and tail)

Skew, Deg 43

r/R	c/D	t/c	P/D	f_m/c
0.2	0.219	0.191	1.319	0.0725
0.3	0.250	0.148	1.366	0.0569
0.4	0.280	0.117	1.408	0.0413
0.5	0.310	0.095	1.445	0.0296
0.6	0.320	0.081	1.477	0.0227
0.7	0.320	0.070	1.503	0.0171
0.8	0.300	0.061	1.517	0.0134
0.9	0.250	0.060	1.509	0.0110
1.0	0.000	0. -	1.475	0. -

TABLE 8 - GEOMETRY OF PROPELLER 4487

Number of Blades 7

Expanded Area Ratio 0.707

Section Meanline NACA a = 0.8

Section Thickness Distribution NACA 66 (DTNSRDC modified nose and tail)

Skew, Deg 43

r/R	c/D	t/c	P/D	f_m/c
0.2	0.163	0.210	1.295	0.0725
0.3	0.184	0.152	1.347	0.0502
0.4	0.206	0.120	1.392	0.0357
0.5	0.222	0.095	1.431	0.0262
0.6	0.231	0.080	1.467	0.0193
0.7	0.229	0.070	1.448	0.0149
0.8	0.214	0.063	1.517	0.0113
0.9	0.239	0.059	1.521	0.0091
1.0	0.000	-	1.508	-

TABLE 9 - GEOMETRY OF PROPELLER 4488

Number of Blades 3

Expanded Area Ratio 0.707

Section Meanline NACA a = 0.8

Section Thickness Distribution NACA 66 (DTNSRDC modified nose and tail)

Skew, Deg 72

r/R	c/D	t/c	P/D	f_m/c
0.2	0.353	0.157	1.475	0.0792
0.3	0.425	0.132	1.475	0.0578
0.4	0.481	0.111	1.474	0.0438
0.5	0.520	0.095	1.489	0.0344
0.6	0.540	0.080	1.506	0.0276
0.7	0.537	0.070	1.519	0.0231
0.8	0.502	0.063	1.519	0.0199
0.9	0.416	0.060	1.501	0.0180
1.0	0.000	-	1.458	-

TABLE 10 - GEOMETRY OF PROPELLER 4489

Number of Blades 3

Expanded Area Ratio 0.709

Section Meanline NACA a = 0.8

Section Thickness Distribution NACA 66 (DTNSRDC modified nose and tail)

Skew, Deg 120

r/R	c/D	t/c	P/D	f_m/c
0.2	0.368	0.200	1.693	0.0816
0.3	0.426	0.152	1.600	0.0635
0.4	0.478	0.119	1.540	0.0510
0.5	0.520	0.098	1.510	0.0425
0.6	0.543	0.082	1.503	0.0354
0.7	0.538	0.069	1.498	0.0300
0.8	0.500	0.061	1.483	0.0258
0.9	0.415	0.058	1.448	0.0233
1.0	0.000	-	1.400	-

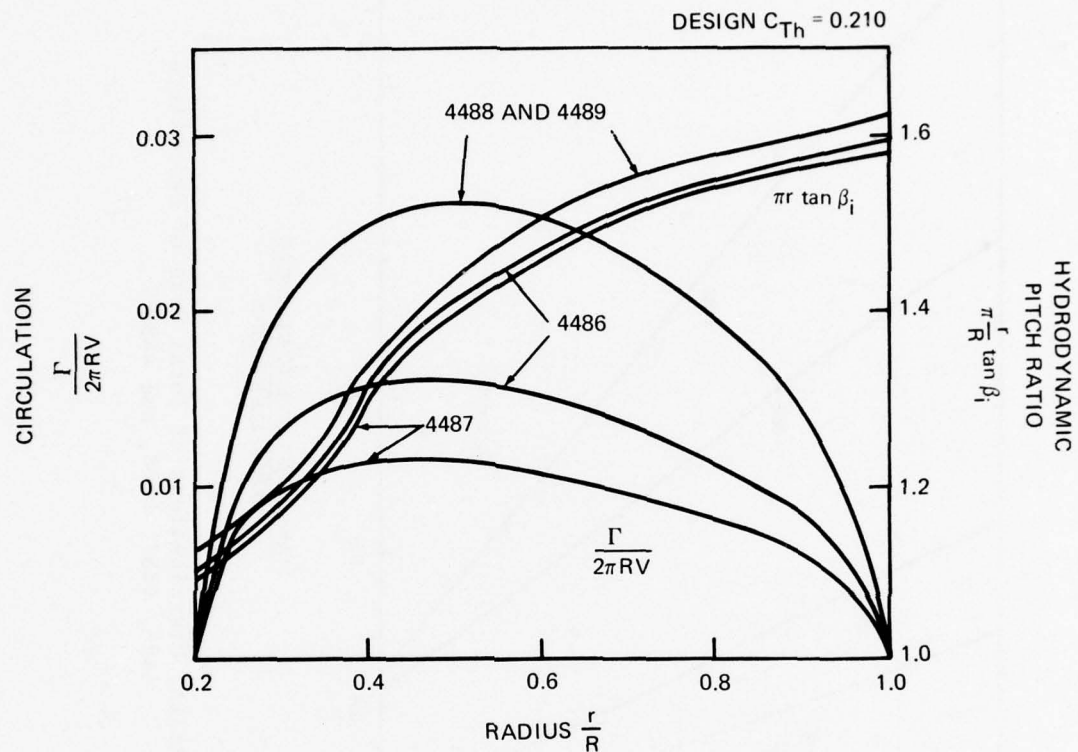


Figure 19 - Lifting Line Circulation and Hydrodynamic Pitch
Representing Loading of Propellers 4486, 4487,
4488, and 4489

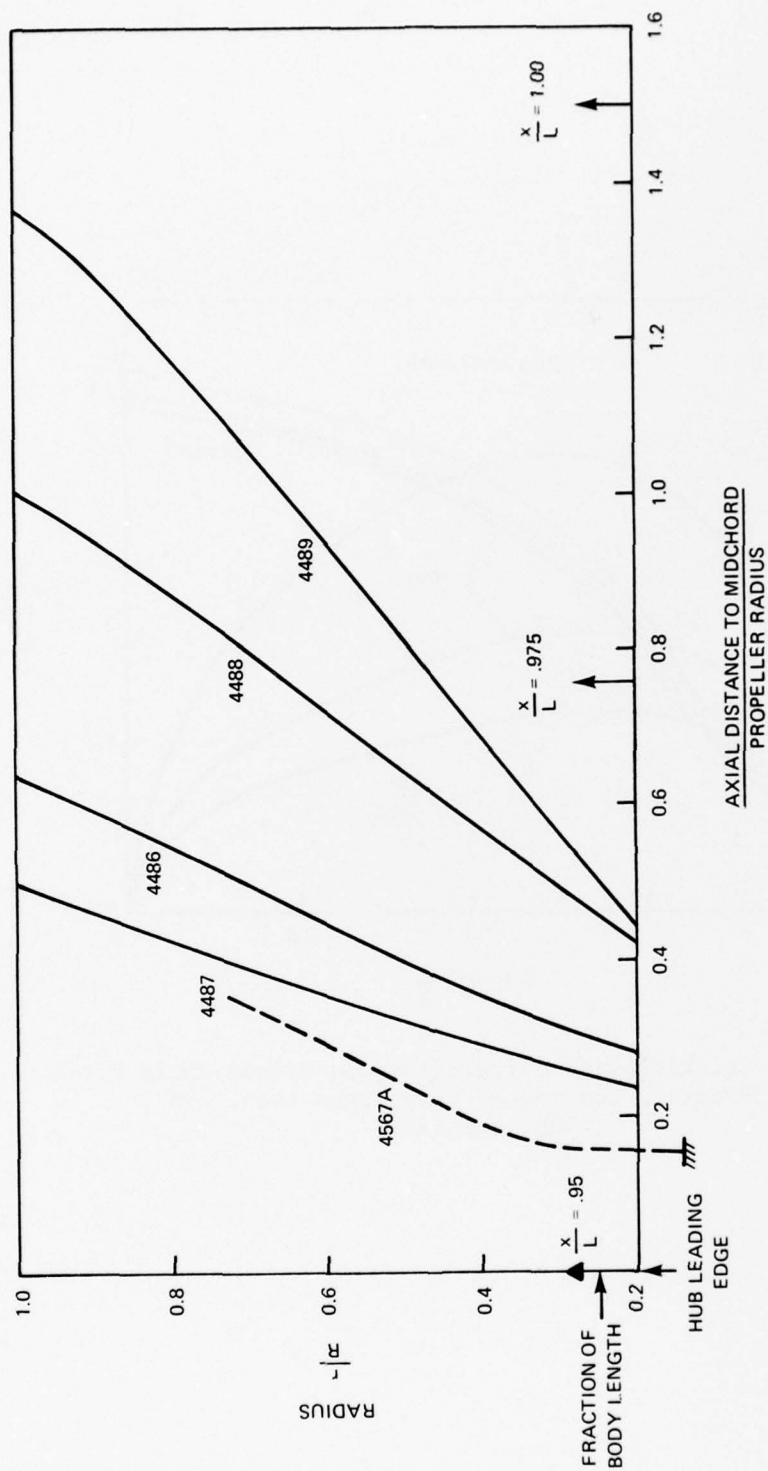


Figure 20 - Radial Distributions of Total Rake of Propellers
4486, 4487, 4488, and 4489

TABLE 11 - COMPUTED* AND MEASURED VALUES OF THRUST DEDUCTION
FRACTION FOR PROPELLERS 4486, 4487, 4488, AND 4489 ON
DTNSRDC MODEL 5224-2

Propeller	$(1-t)_{\text{Experiment}}$	$(1-t)_{\text{Theory}}$	t_{Body}	$t_{\text{Appendages}}$
4486	0.909	0.949	0.039	0.012
4487	0.891	0.941	0.045	0.014
4488	0.936	0.966	0.027	0.007
4489	0.964	0.974	0.021	0.005

*Without corrections for increased frictional resistance

By considering the longitudinal distribution of thrust deduction (body only) shown in Figure 21, it may be concluded that virtually all of the interaction force develops on the last 20 percent of the body. Within this region the effect of rake is manifested as a change in propeller induced velocities. The total axial induced velocity on the afterbody is shown in Figure 22. The separate lifting line and lifting surface contributions are displayed in Figure 23, showing corrections for skew and rake to the essential difference.

The effect of blade thickness is to decelerate the flow ahead of the propeller and hence, reduce the interaction force. In the present example, this effect is more pronounced even for the least raked propeller (4487) because of the relative *volume* of each blade compared to the loading. For propellers of equal blade volume, the influence of thickness would diminish with increasing rake. Such is not the case here because, for increased rake, more material is required for equal strength. Thus propeller 4489, while raked the most, also has the largest thickness contribution because of blade volume (for example, it is approximately twice the volume of propeller 4487).

CONCLUSIONS AND RECOMMENDATIONS

An improved theory and computer-aided numerical analysis have been developed for predicting the added resistance (thrust deduction) arising from the propeller-hull interaction. The theory is formulated in terms of the diffracted potential flow about the hull in the presence of the propeller-induced velocity field. The propeller representation is derived from lifting-surface theory which includes the effects of blade thickness, skew, rake, and chordwise load distribution. It is shown that these effects may be regarded as corrections to the moderately-loaded lifting-line (sink disk) approximation.

Important features of the analysis and comparisons with experimental results are illustrated by application to several stern propeller-appended body-of-revolution configurations. Based on these sample calculations, the following conclusions are drawn:

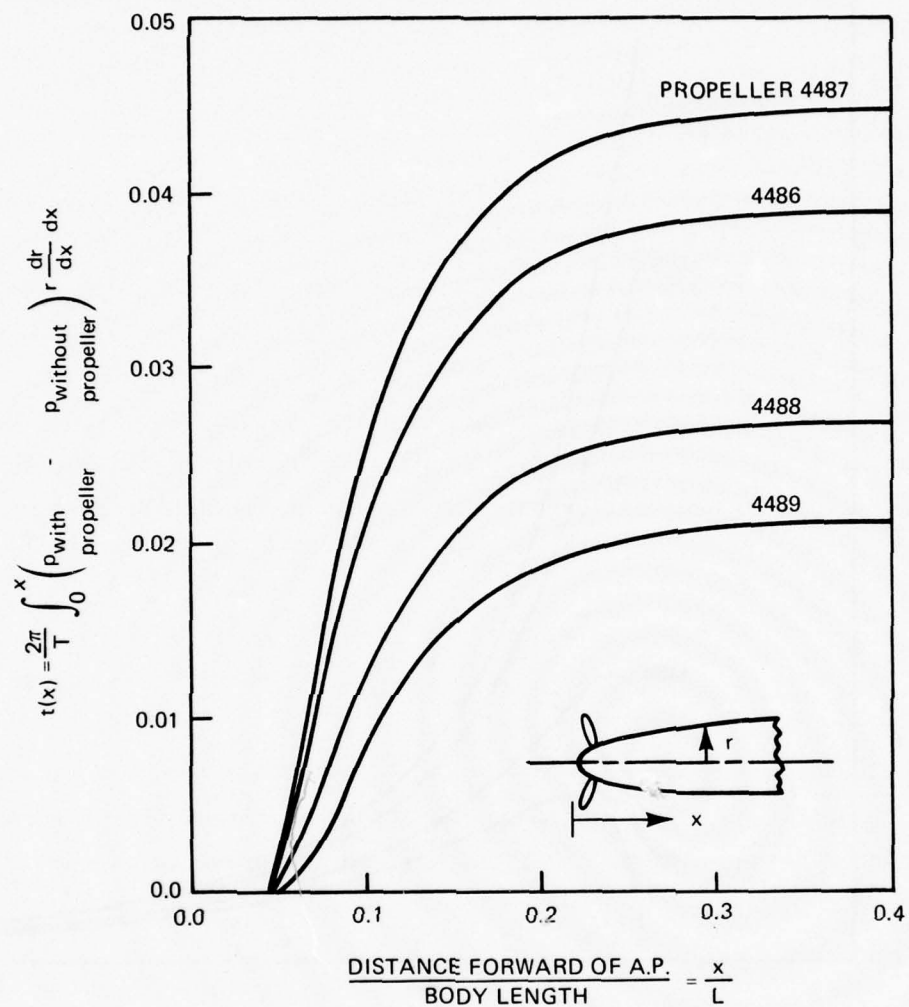


Figure 21 - Longitudinal Distribution of Thrust Deduction (Cumulative From Stern) With Four Propellers on Body 5224-2

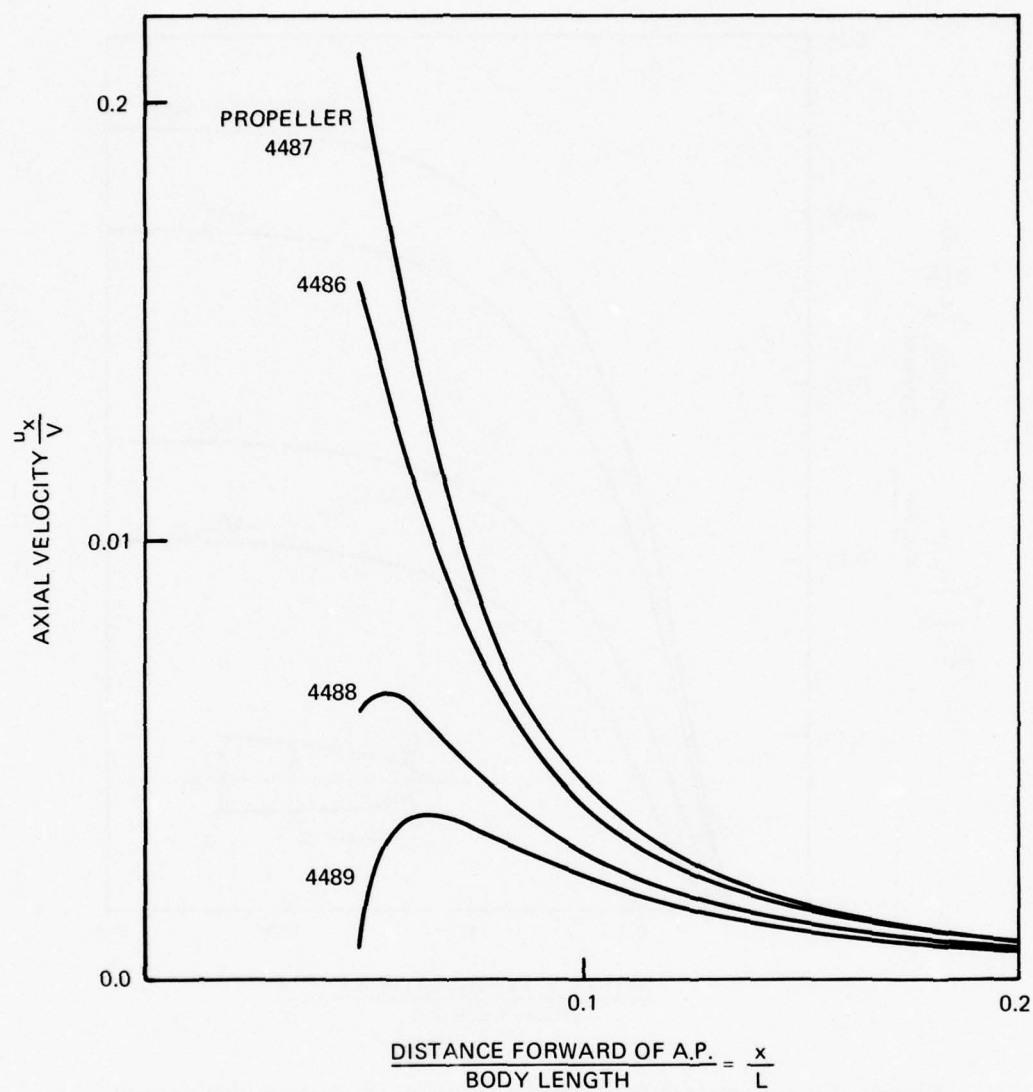


Figure 22 - Propeller Induced Axial Velocities on Appended Body of Revolution 5224-2

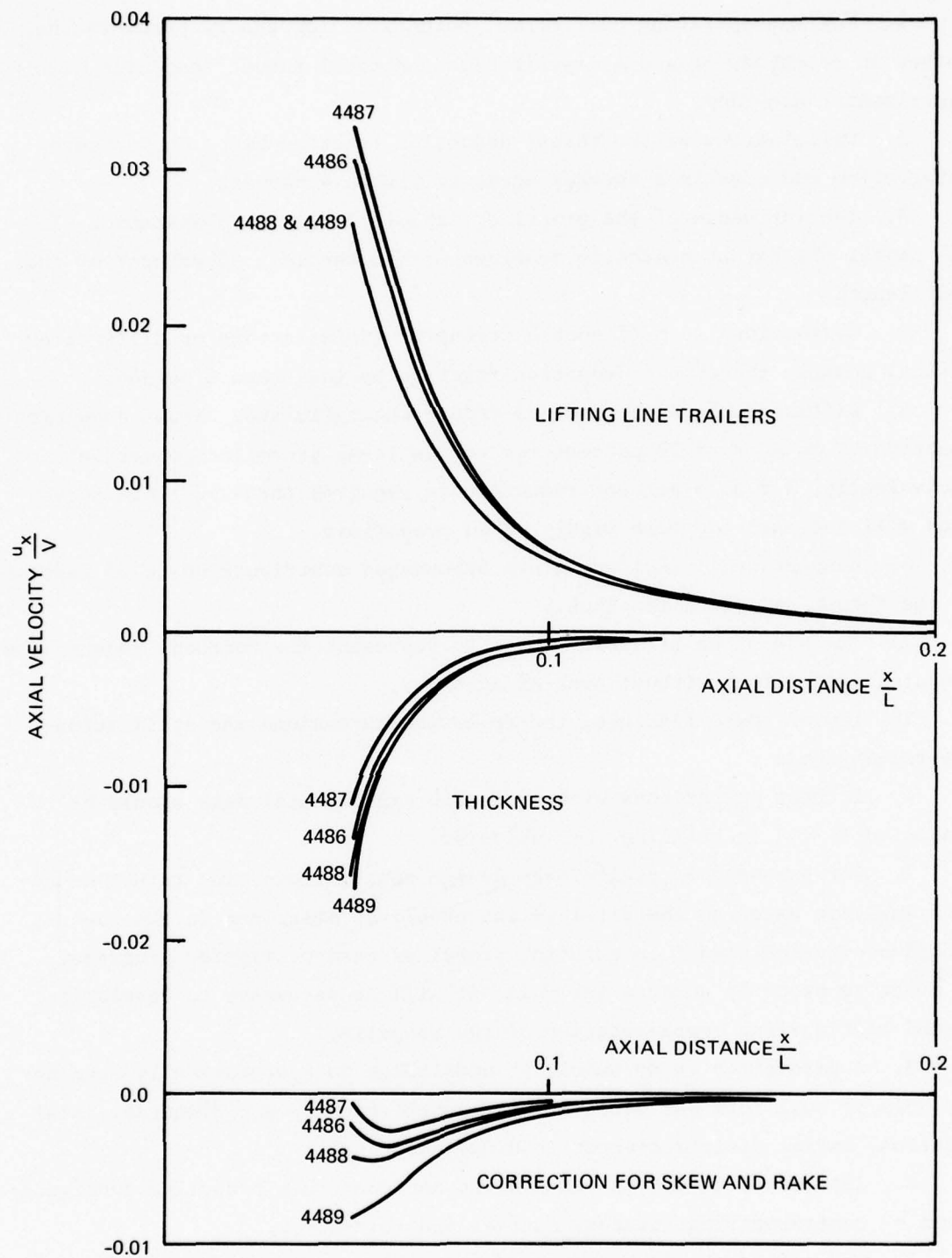


Figure 23 - Contributions to Propeller Induced Axial Velocity on Body 5224-2

1. For nonseparating hull forms, potential flow theory predicts the change in afterbody pressure distribution and total thrust deduction within experimental accuracy.

2. Calculations of the thrust deduction fraction based on pressure integration and Lagally's theorem agree to within 4 percent.

3. The influence of the propeller rapidly decays with distance. In all cases, the thrust deduction develops within the last 30 percent of the hull length.

4. Corrections to hull source strengths (interference or diffraction effect) changes the thrust deduction fraction by less than 3 percent.

5. Lifting-surface corrections reduce the calculated thrust deduction fraction by as much as 20 percent for conventional propeller geometries (or equivalently, a 2 to 3 percent reduction in required thrust). This correction will increase for more highly raked propellers.

6. Conventional cruciform stern appendages contribute up to 25 percent of the thrust deduction fraction.

7. The use of an afterbody image to represent the forebody reduces the computational effort without loss of accuracy.

In view of these findings, the following extensions and applications are recommended:

1. Further comparisons with available experimental data should be conducted to aid in refining the analysis.

2. For purposes of preliminary design calculations, the thrust deduction analysis based on the lifting-line model, as described in the report, should be incorporated into existing propeller design computer programs. In order to properly account for rake, it will be necessary to develop a curved lifting-line representation of the propeller.

3. A parametric study should be undertaken to systematically examine the role of hull form and propeller characteristics (e.g., diameter, axial location, radial distribution of loading, and rake).

4. The method should be extended to include other propeller configurations -- contrarotating, tandem, ducted, and twin-screw.

5. The method should be extended to apply to surface-ship configurations.

ACKNOWLEDGMENTS

The authors are indebted to a number of people for their assistance in the course of this work. Mr. T.A. LaFone, Mr. J. Diskin, and Ms. R.B. Hurwitz aided in the development and execution of the various computer programs. Mr. C. Dawson and Ms. J. Dean provided invaluable guidance in the use of the XYZ potential-flow computer program. Finally, the authors wish to thank Messrs. J. McCarthy, T. Huang, and H. Wang for their continued interest in the analytical work and support in obtaining experimental data presented in this report.

REFERENCES

1. Nowacki, H. and S.D. Sharma, "Free Surface Effects in Hull Propeller Interaction," The University of Michigan College of Engineering Report 112 (Sep 1971).
2. Dickmann, H.E., "The Interaction between Propeller and Ship with Special Consideration to the Influence of Waves," Jahrbuch der Schiffbautechnischen Gesellschaft, Vol. 40 (1939).
3. Weinblum, G., "The Thrust Deduction," American Society of Naval Engineers, Vol. 63 (1951).
4. Korvin-Kroukovsky, B.V., "Stern Propeller Interaction with a Streamline Body of Revolution," International Shipbuilding Progress, Vol. 3, No. 17 (1956).
5. Beveridge, J.L., "Pressure Distribution on Towed and Propelled Streamline Bodies of Revolution at Deep Submergence," David Taylor Model Basin Report 1665 (Jun 1966).
6. Beveridge, J.L., "Analytical Prediction of Thrust Deduction for Submersibles and Surface Ships," Journal of Ship Research, Vol. 13, No. 4 (Dec 1969).
7. Nelson, D.M., "Development and Application of a Lifting-Surface Design Method for Counterrotating Propellers," Naval Undersea Center TP 326 (Nov 1972).
8. Beveridge, J.L., "Thrust Deduction in Contrarotating Propellers," Naval Ship Research and Development Center Report 4332 (Nov 1974).
9. Huang, T. et al., "Propeller/Stern/Boundary-Layer Interaction on Axisymmetric Bodies: Theory and Experiment," DTNSRDC Report 76-0113 (Dec 1976).
10. Hess, J.L. and A.M.O. Smith, "Calculation of Nonlifting Potential Flow About Arbitrary Three-Dimensional Bodies," Journal of Ship Research (Sep 1964).
11. Hess, J.L. and A.M.O. Smith, "Calculation of Potential Flow About Arbitrary Bodies," Pergamon Press, Progress in Aeronautical Sciences, Vol. 8 (1966).
12. Dawson, C.W. and J.S. Dean, "The XYZ Potential Flow Program," NSRDC Report 3892 (Jun 1972).
13. Cummins, W.E., "The Force and Moment on a Body in a Time-Varying Potential Flow," Journal of Ship Research, Vol. 1, No. 1 (Apr 1957).
14. Milne-Thomson, L.M., "Theoretical Hydrodynamics," The Macmillan Company, New York, N.Y., 2nd edition (1950).
15. Kerwin, J.E. and R. Leopold, "A Design Theory for Subcavitating Propellers," Transactions SNAME, Vol. 72 (1964).
16. Kerwin, J.E., "Computer Technique for Propeller Blade Section Design," International Shipbuilding Progress, Vol. 20, No. 227 (Jul 1973).

17. Denny, S.B., "Comparisons of Experimentally Determined and Theoretically Predicted Pressures in the Vicinity of a Marine Propeller," Naval Ship Research and Development Center Report 2349 (May 1967).
18. Lerbs, H.W., "Moderately Loaded Propellers with Finite Numbers of Blades and an Arbitrary Distribution of Circulation," Transactions SNAME, Vol. 60 (1952).
19. Morgan, W.B. and J.W. Wrench, "Some Computational Aspects of Propeller Design," Methods in Computational Physics, Vol. 4, Academic Press Inc., New York, N.Y. (1965).
20. Wu, T.Y., "Some Recent Developments in Propeller Theory," Schiffstechnik, Vol. 9, No. 47 (1962).
21. Cummings, D.E., "Numerical Prediction of Propeller Characteristics," Journal of Ship Research, Vol. 17, No. 1 (Mar 1973).
22. Tsao, S.S., "Documentation of Programs for the Analysis of Performance and Spindle Torque of Controllable Pitch Propellers," Mass. Inst. of Technology, Dept of Ocean Engineering, Report No. 75-8 (May 1975).
23. Landweber, L. and M. Gertler, "Mathematical Formulation of Bodies of Revolution," DTMB Report 719 (Sept 1950).
24. Brockett, T., "Minimum Pressure Envelopes for Modified NACA-66 Sections with NACA $a = .8$ Camber and BUSHIPS Type I and II Sections," DTNSRDC Report 1780 (Feb 1966).

APPENDIX A

THE FORCE GENERATED ON A BODY IN POTENTIAL FLOW BY AN ISOLATED SINGULARITY

Consider a body immersed in a uniform stream, \vec{V}_∞ , with an isolated point singularity located external to the body at $\vec{r} = \vec{r}_Q$. The flow is assumed to be steady, irrotational, and incompressible. If the body is represented by a surface distribution of source singularities $\sigma(\vec{r}_B)$, then the force exerted on the body is given by (Equation (13) in the text)

$$\vec{F} = - \rho \oint_{S_B} \sigma(\vec{r}_B) \vec{v}_Q(\vec{r}_B) dS(\vec{r}_B)$$

where $\vec{v}_Q(\vec{r}_B)$ is the velocity induced by the singularity at the body surface. This relation may be derived by considering the control volume illustrated in Figure A-1.

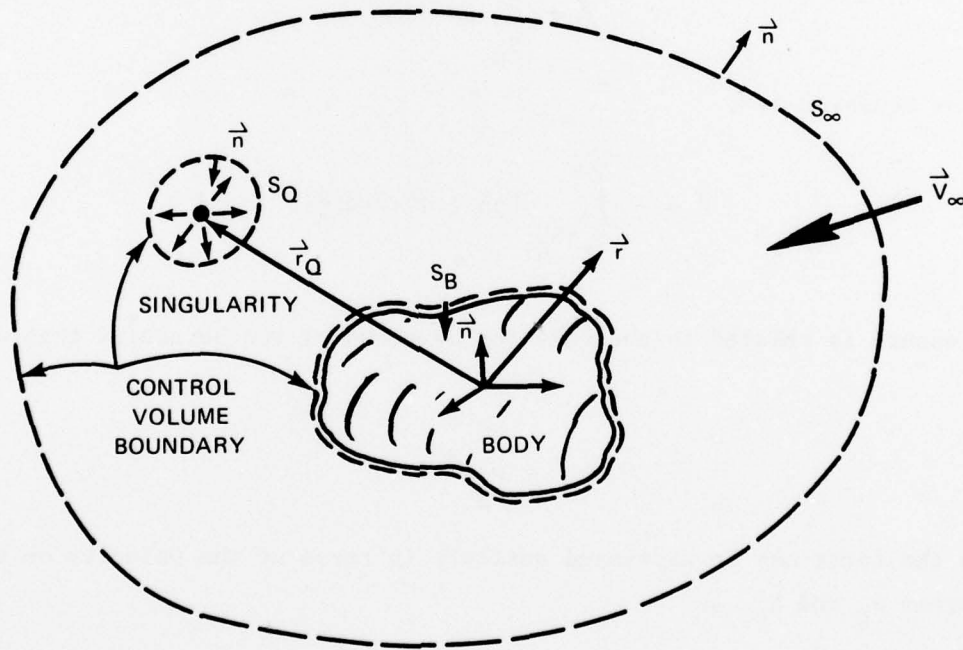


Figure A-1 - Control Volume for Analysis of Force on Body

The pressure forces acting on the control volume surface are equal to the time rate of change of linear momentum, \vec{M} , of the fluid within the control volume. For steady incompressible flow, one obtains

$$\begin{aligned}
 - \oint_{S_{\infty} + S_B + S_Q} (p\vec{n}) dS &= \frac{D}{Dt} \int_{\text{Control volume C.V.}} \vec{M} dV \\
 &= \frac{D}{Dt} \int_{\text{C.V.}} \rho \vec{V} dV \\
 &= \rho \int_{\text{C.V.}} \vec{V} \cdot \nabla \vec{V} dV \\
 &= \rho \int_{S_{\infty} + S_Q + S_B} \vec{V} (\vec{V} \cdot \vec{n}) dS
 \end{aligned} \tag{A-1}$$

On the body surface, it is required that $\vec{V} \cdot \vec{n} = 0$. The force acting on the body is

$$\vec{F} = \int_{S_B} p\vec{n} dS$$

or, from Equation A-1,

$$\vec{F} = - \int_{S_{\infty} + S_Q} [p\vec{n} + \rho \vec{V} (\vec{V} \cdot \vec{n})] dS$$

The pressure is related to the velocity by means of the Bernoulli theorem as

$$p = - \rho \frac{\vec{V} \cdot \vec{V}}{2}$$

and so the force may be expressed entirely in terms of the velocity on the boundaries S_Q and S_{∞} , as

$$\vec{F} = \int_{S_Q + S_{\infty}} \left[\frac{\rho}{2} (\vec{V} \cdot \vec{V}) \vec{n} - \rho \vec{V} (\vec{V} \cdot \vec{n}) \right] dS \tag{A-2}$$

It is now necessary to develop expressions for the velocity at large distances ($|\vec{r}| \rightarrow \infty$) and in the immediate vicinity of the singularity ($\vec{r} - \vec{r}_Q \rightarrow 0$). For convenience, the velocity may be regarded as the sum of three terms,

$$\vec{V}(\vec{r}) = \underbrace{\vec{V}_\infty}_{\substack{\text{Free} \\ \text{Stream} \\ \text{Velocity}}} + \underbrace{\vec{V}_B(\vec{r})}_{\substack{\text{Body} \\ \text{Induced} \\ \text{Velocity}}} + \underbrace{\vec{V}_Q(\vec{r})}_{\substack{\text{Singularity} \\ \text{Induced} \\ \text{Velocity}}}$$

The body velocity, $\vec{V}_B(\vec{r})$, is given by

$$\vec{V}_B(\vec{r}) = \frac{1}{4\pi} \int_{S_B} \sigma(\vec{r}_B) \frac{\vec{r} - \vec{r}_B}{|\vec{r} - \vec{r}_B|^3} dS(\vec{r}_B)$$

As $|\vec{r}| \rightarrow \infty$,

$$\vec{V}_B(\vec{r}) \sim \frac{-\vec{\mu}_B}{4\pi |\vec{r}|^3} + \frac{1}{4\pi} \frac{3\vec{r}(\vec{\mu}_B \cdot \vec{r})}{|\vec{r}|^5} + O\left(\frac{1}{|\vec{r}|^4}\right)$$

where

$$\vec{\mu}_B = \int_{S_B} \sigma(\vec{r}_B) \vec{r}_B dS(\vec{r}_B)$$

As $\vec{r} \rightarrow \vec{r}_Q$,

$$\vec{V}_B(\vec{r}) \sim \vec{V}_B(\vec{r}_Q) - \epsilon \vec{n} \cdot \nabla_{\vec{r}_Q} \vec{V}_B(\vec{r}_Q) + O(\epsilon^2)$$

where

$$\epsilon \vec{n} = \vec{r}_Q - \vec{r}$$

If the singularity is a point source of strength m , then

$$\vec{V}_Q(\vec{r}) = \frac{m}{4\pi} \frac{\vec{r} - \vec{r}_Q}{|\vec{r} - \vec{r}_Q|^3}$$

Then, as $|\vec{r}| \rightarrow \infty$,

$$\vec{V}_Q(\vec{r}) \sim \frac{m}{4\pi} \frac{\vec{r}}{|\vec{r}|^3} + \frac{3m}{4\pi} \frac{\vec{r}(\vec{r}_Q \cdot \vec{r})}{|\vec{r}|^5} - \frac{m \vec{r}_Q}{4\pi |\vec{r}|^3} + O\left(\frac{1}{|\vec{r}|^4}\right)$$

and as $\vec{r} \rightarrow \vec{r}_Q$

$$\vec{V}_Q(\vec{r}) = -\frac{m}{4\pi} \frac{\vec{n}}{\epsilon^2}$$

If these expressions are inserted into Equation A-2, the following results are obtained by carefully evaluating the limits

$$\begin{aligned} \vec{F} &= \int_{S_\infty} \vec{V} dS + \int_{S_{Q_\epsilon}} \vec{V} dS \\ &= -\rho \vec{V}_\infty m + \rho m [\vec{V}_\infty + \vec{V}_B(\vec{r}_Q)] \\ &= \rho m \vec{V}_B(\vec{r}_Q) \\ &= \frac{\rho m}{4\pi} \oint_{S_B} \sigma(\vec{r}_B) \frac{\vec{r}_Q - \vec{r}_B}{|\vec{r}_Q - \vec{r}_B|^3} dS(\vec{r}_B) \\ &= -\rho \oint_{S_B} \sigma(\vec{r}_B) \left\{ \frac{m}{4\pi} \frac{\vec{r}_B - \vec{r}_Q}{|\vec{r}_B - \vec{r}_Q|^3} \right\} dS(\vec{r}_B) \end{aligned}$$

or

$$\vec{F} = - \rho \oint_{S_B} \sigma(\vec{r}_B) \vec{V}_Q(\vec{r}_B) dS(\vec{r}_B)$$

which is the desired result. The solution for the case of a doublet singularity may also be written in this form, although the derivation is considerably more involved.

APPENDIX B

SINK DISK REPRESENTATION OF A MODERATELY LOADED PROPELLER

The circumferential mean axial and radial velocities induced by a moderately loaded propeller (outside the slipstream) can be related to the flow generated by a sink disk. Consider the velocity potential associated with a distribution of sources, $\sigma(r, \varphi)$, located at the propeller plane $x = 0$, $0 \leq r \leq R$,

$$\phi(x, r, \varphi) = -\frac{1}{4\pi} \int_0^{2\pi} \int_0^R \frac{\sigma(r', \varphi') r' dr' d\varphi'}{\sqrt{x^2 + r^2 + r'^2 - 2rr' \cos(\varphi - \varphi')}}.$$

If the source strengths are independent of angular position, φ , the integral may be rewritten as

$$\phi(x, r) = -\frac{1}{2} \int_0^R \sigma(r') \int_0^\infty dk J_0(kr) J_0(kr') e^{-k|x|} dk dr'$$

Integrating by parts yields

$$\phi(x, r) = \frac{1}{2} \int_0^R r' \frac{d\sigma(r')}{dr'} \int_0^\infty dk \frac{J_0(kr) J_1(kr')}{k} e^{-k|x|} dk dr'$$

where it is required that $\sigma(R) = 0$. The axial and radial velocities are then given by

$$\frac{\partial \phi}{\partial x}(x, r) = \pm \frac{1}{2} \int_0^R r' \frac{d\sigma(r')}{dr'} \int_0^\infty J_0(kr) J_1(kr') e^{-k|x|} dk dr' \quad x \gtrless 0$$

$$\frac{\partial \phi}{\partial r}(x, r) = \frac{1}{2} \int_0^R r' \frac{d\sigma(r')}{dr'} \int_0^\infty J_1(kr) J_1(kr') e^{-k|x|} dk dr' \quad \text{all } x$$

These results are equivalent to the induced velocities of the propeller (Equation (26) in text) provided that

$$\frac{d\sigma(r)}{dr} = 0 \quad r < R_H$$

$$\frac{d\sigma(r)}{dr} = -\frac{Z}{2\pi} \frac{d\Gamma(r)}{dr} \frac{1}{r \tan \beta_i(r)} \quad R_H \leq r \leq R$$

It follows that

$$\sigma(r) = \frac{Z}{2\pi} \int_r^R \frac{d\Gamma(r')}{dr'} \frac{dr'}{r' \tan \beta_i(r')}$$

where the constant of integration is set so that $\sigma(R) = 0$. For typical propeller loading distributions, $\sigma(r)$ is negative over most of the disk, corresponding to a sink distribution.

INITIAL DISTRIBUTION

Copies

- 1 WES
- 1 U.S. ARMY TRAS R&D
Marine Trans Div
- 1 CHONR/438 Cooper
- 2 NRL
 - 1 Code 2027
 - 1 Code 2629
- 1 ONR/Boston
- 1 ONR/Chicago
- 1 ONR/New York
- 1 ONR/Pasadena
- 1 ONR/San Francisco
- 1 NORDA
- 3 USNA
 - 1 Tech Lib
 - 1 Nav Sys Eng Dept
 - 1 B. Johnson
- 3 NAVPGSCOL
 - 1 Library
 - 1 T. Sarpkaya
 - 1 J. Miller
- 1 NADC
- 4 NOSC, San Diego
 - 1 Library
 - 1 T. Lang
 - 1 J.W. Hoyt
 - 1 D.M. Nelson
- 1 NCSL/712 D. Humphreys
- 1 NCEL/Code 131
- 1 NSWC, White Oak/Lib
- 1 NSWC, Dahlgren/Lib
- 1 NUSC/Lib
- 7 NAVSEA
 - 1 SEA 0322
 - 1 SEA 033
 - 1 SEA 03512/Peirce
 - 1 SEA 037
 - 3 SEA 09G32
- 1 NAVFAC/Code 032C

Copies

- 1 NAVSHIPYD PTSMH/Lib
- 1 NAVSHIPYD PHILA/Lib
- 1 NAVSHIPYD NORVA/Lib
- 1 NAVSHIPYD CHASN/Lib
- 1 NAVSHIPYD LBEACH/Lib
- 2 NAVSHIPYD MARE
 - 1 Library
 - 1 Code 250
- 1 NAVSHIPYD BREM/Lib
- 1 NAVSHIPYD PEARL/Code 202.32
- 8 NAVSEC
 - 1 SEC 6034B
 - 1 SEC 6110
 - 1 SEC 6114H
 - 1 SEC 6120
 - 1 SEC 6136
 - 1 SEC 6140B
 - 1 SEC 6144
 - 1 SEC 6148
- 1 NAVSEC, NORVA/6660.03 Blount
- 12 DDC
- 1 AFOSR/NAM
- 1 AFFOL/FYS, J. Olsen
- 2 MARAD
 - 1 Div of Ship R&D
 - 1 Lib
- 1 NASA HQS/Lib
- 3 NBS
 - 1 Lib
 - 1 P.S. Klebanoff
 - 1 G. Kulin
- 1 NSF/Eng Lib
- 1 LC/Sci & Tech
- 1 DOT/Lib TAD-491.1
- 2 MMA
 - 1 National Maritime Research Cntr
 - 1 Library
- 1 U. of Bridgeport/E. Uram

Copies

- 4 U. of Cal/Dept Naval Arch,
Berkeley
 - 1 Library
 - 1 W. Webster
 - 1 J. Paulling
 - 1 J. Wehausen
- 2 U. of Cal, San Diego
 - 1 A.T. Ellis
 - 1 Scripps Inst Lib
- 5 CIT
 - 1 Aero Lib
 - 1 T.Y. Wu
 - 1 A.J. Acosta
 - 1 I. Sabersky
 - 1 D. Coles
- 1 Catholic U. of Amer./Civil &
Mech Eng
- 1 Colorado State U./Eng Res Cen
- 1 U. of Connecticut/Scottron
- 1 Cornell U./Shen
- 2 Florida Atlantic U.
 - 1 Tech Lib
 - 1 S. Dunne
- 2 Harvard U.
 - 1 G. Carrier
 - 1 Gordon McKay Lib
- 1 U. of Hawaii/Bretschneider
- 1 U. of Illinois/J. Robertson
- 4 U. of Iowa
 - 1 Library
 - 1 L. Landweber
 - 1 J. Kennedy
 - 1 V.C. Patel
- 1 Johns Hopkins U./Phillips
- 1 Kansas State U./Nesmith
- 1 U. of Kansas/Civil Eng Lib
- 1 Lehigh U./Fritz Eng Lab Lib
- 6 MIT
 - 1 Library
 - 1 P. Leehey
 - 1 P. Mandel
 - 1 M. Abkowitz
 - 1 J.N. Newman
 - 1 J.E. Kerwin

Copies

- 4 U. of Minn/St. Anthony Falls
 - 1 Silberman
 - 1 Lib
 - 1 Song
 - 1 R. Arndt
- 5 U. of Mich/NAME
 - 1 Library
 - 1 F. Ogilvie
 - 1 Hammitt
 - 1 Couch
 - 1 W. Vorus
- 2 U. of Notre Dame
 - 1 Eng Lib
 - 1 Strandhagen
- 2 New York U./Courant Inst
 - 1 A. Peters
 - 1 J. Stoker
- 4 Penn State
 - 1 B.R. Parkin
 - 1 R.E. Henderson
 - 1 ARL Lib
 - 1 W. Gearhart
- 1 Princeton U./Mellor
- 2 U. of Rhode Island
 - 1 F.M. White
 - 1 T. Kowalski
- 6 SIT
 - 1 Library
 - 1 Breslin
 - 1 Savitsky
 - 1 P.W. Brown
 - 1 Tsakonas
 - 1 Valentine
- 1 U. of Texas/Arl Lib
- 1 Utah State U./Jeppson
- 2 Southwest Res Inst
 - 1 Applied Mech Rev
 - 1 Abramson
- 3 Stanford U.
 - 1 Eng Lib
 - 1 R. Street, Dept Civil Eng
 - 1 S.J.Kline, Dept Mech Eng
- 1 Stanford Res Inst/Lib
- 1 U. of Washington/Arl Tech Lib

Copies

- 3 VPI
 - 1 H.L. Moses, Dept Mech Eng
 - 1 D.P. Telionis, Dept Mech Eng
 - 1 J. Schetz, Dept Aero & Ocean Eng
- 3 Webb Inst
 - 1 Library
 - 1 Lewis
 - 1 Ward
- 1 Woods Hole/Ocean Eng
- 1 Worchester PI/Tech Lib
- 1 SNAME/Tech Lib
- 1 Bethlehem Steel/Sparrows Point
- 1 Bethlehem Steel/New York/Lib
- 1 Bolt, Beranek & Newman/Lib
- 1 Exxon, NY/Design Div, Tank Dept
- 1 Exxon Math & System, Inc.
- 1 General Dynamics, EB/Boatwright
- 1 Gibbs & Cox/Tech Info

Copies

- 4 Hydronautics
 - 1 Library
 - 1 E. Miller
 - 1 V. Johnson
 - 1 C.C. Hsu
- 1 Lockheed, Sunnyvale/Waid
- 2 McDonnell Douglas, Long Beach
 - 1 T. Cebeci
 - 1 J. Hess
- 1 Newport News Shipbuilding/Lib
- 1 Nielsen Eng & Res
- 1 Oceanics
- 3 Rand Corp
 - 1 E.R. Van Driest
 - 1 C. Gazley
 - 1 J. Aroesty
- 1 Rockwell International/B. Ujihara
- 1 Sperry Rand/Tech Lib
- 1 Sun Shipbuilding/Chief Naval Arch
- 1 Robert Taggart
- 1 Tracor
- 3 Westinghouse Electric
 - 1 M.S. Macovsky
 - 1 Gulino
 - 1 Mons
- 1 J. Beveridge

CENTER DISTRIBUTION

Copies	Code		Copies	Code	
1	012	R.C. Allen	1	1552	M. Chang
1	11	W.M. Ellsworth	1	1552	T.T. Huang
1	117	R.M. Stevens	1	1552	H.T. Wang
1	1500	W.E. Cummins	1	1552	Brockett
1	1504	V.J. Monacella	1	1552	J. McCarthy
1	1506	M.K. Ochi	1	1560	G. Hagen
1	1507	D. Cieslowski	1	1562	M. Martin
1	1508	F. Peterson	1	1564	J. Feldman
1	1512	J.B. Hadler	1	1568	G. Cox
1	152	R. Wermter	1	1572	M.D. Ochi
1	1521	P. Pien	1	1572	E. Zarnick
1	1524	Y.T. Shen	1	1572	C.M. Lee
1	1524	W.C. Lin	1	1576	W.E. Smith
1	1524	Day	1	1615	R.J. Furey
1	1524	Scragg	1	1802.2	F. Frenkiel
1	1532	G. Dobay	1	183	E. Cuthill
1	1532	M. Wilson	1	184	H. Lugt
1	154	W.B. Morgan	1	1843	J. Schot
1	1541	Granville	1	1843	C. Dawson
1	1542	Yim	1	19	M.M. Sevik
1	1544	Cumming			
1	1544	Boswell			
1	1544	Caster	30	5214.1	Reports Distribution
30	1544	Cox	1	522.1	Unclassified Library (C)
1	1544	Jessup	1	522.2	Unclassified Library (A)

DTNSRDC ISSUES THREE TYPES OF REPORTS

- 1. DTNSRDC REPORTS, A FORMAL SERIES, CONTAIN INFORMATION OF PERMANENT TECHNICAL VALUE. THEY CARRY A CONSECUTIVE NUMERICAL IDENTIFICATION REGARDLESS OF THEIR CLASSIFICATION OR THE ORIGINATING DEPARTMENT.**
- 2. DEPARTMENTAL REPORTS, A SEMIFORMAL SERIES, CONTAIN INFORMATION OF A PRELIMINARY, TEMPORARY, OR PROPRIETARY NATURE OR OF LIMITED INTEREST OR SIGNIFICANCE. THEY CARRY A DEPARTMENTAL ALPHANUMERICAL IDENTIFICATION.**
- 3. TECHNICAL MEMORANDA, AN INFORMAL SERIES, CONTAIN TECHNICAL DOCUMENTATION OF LIMITED USE AND INTEREST. THEY ARE PRIMARILY WORKING PAPERS INTENDED FOR INTERNAL USE. THEY CARRY AN IDENTIFYING NUMBER WHICH INDICATES THEIR TYPE AND THE NUMERICAL CODE OF THE ORIGINATING DEPARTMENT. ANY DISTRIBUTION OUTSIDE DTNSRDC MUST BE APPROVED BY THE HEAD OF THE ORIGINATING DEPARTMENT ON A CASE-BY-CASE BASIS.**